MCPH1 inhibits condensin II during interphase by regulating its SMC2-kleisin interface

Martin Houlard[†1], Erin E. Cutts[†2], Muhammad S. Shamim[3,4,5], Jonathan Godwin[1], David Weisz[3,5], Aviva Presser Aiden[3,5], Erez Lieberman Aiden[3,5], Lothar Schermelleh[1], Alessandro Vannini[2,6*], Kim Nasmyth[1*]

[†]These authors contributed equally.

1. Department of Biochemistry, University of Oxford, United Kingdom
2. Division of Structural Biology, The Institute of Cancer Research, London, United Kingdom.
3. The Center for Genome Architecture, Department of Molecular and Human Genetics, Baylor College of Medicine, Houston, TX 77030
4. Medical Scientist Training Program, Baylor College of Medicine, Houston, TX 77030, USA. 4 Department of Bioengineering, Rice University, Houston, TX 77030, USA.
5. Center for Theoretical Biological Physics, Rice University, Houston, TX 77005, USA.
6. Fondazione Human Technopole, Structural Biology Research Centre, Milan, Italy

*To whom correspondence should be addressed: ashley.nasmyth@bioch.ox.ac.uk and alessandro.vannini@fht.org

ABSTRACT:

The dramatic change in morphology of chromosomal DNAs between interphase and mitosis is one of the defining features of the eukaryotic cell cycle. Two types of enzymes, namely cohesin and condensin confer the topology of chromosomal DNA by extruding DNA loops. While condensin normally configures chromosomes exclusively during mitosis, cohesin does so during interphase. The processivity of cohesin's LE during interphase is limited by a regulatory factor called WAPL, which induces cohesin to dissociate from chromosomes via a mechanism that requires dissociation of its kleisin from the neck of SMC3. We show here that a related mechanism may be responsible for blocking condensin II from acting during interphase. Cells from patients carrying mutations in the *Mcph1* gene undergo premature chromosome condensation but it has never been established for certain whether MCPH1 regulates condensin II directly. We show that deletion of *Mcph1* in mouse embryonic stem cells unleashes an activity of condensin II that triggers formation of compact chromosomes in G1 and G2 phases, which is accompanied by enhanced mixing of A and B chromatin compartments, and that this occurs even in the absence of CDK1 activity. Crucially, inhibition of condensin II by MCPH1 depends on the binding of a short linear motif within MCPH1 to condensin II's NCAPG2 subunit. We show that the activities of both Cohesin and Condensin II may be restricted during interphase by similar types of mechanisms as MCPH1's ability to block condensin II's association with chromatin is abrogated by the fusion of SMC2 with NCAPH2. Remarkably, in the absence of both WAPL and MCPH1, cohesin and condensin II transform chromosomal DNAs of G2 cells into chromosomes with a solenoidal axis showing that both SMC complexes must be tightly regulated to adjust both the chromatid's structure and their segregation.

INTRODUCTION

The segregation of sister DNAs during mitosis requires that they are first disentangled and organised into individual sister chromatids before being pulled in opposite directions by the mitotic spindle upon the dissolution of sister chromatid cohesion by separase. Chromatid formation during mitosis and sister chromatid cohesion necessary for bi-orientation are mediated by highly related structural maintenance of chromosomes (SMC)-kleisin complexes, namely condensin and cohesin respectively. In both cases, the activity of their ring-like SMC-kleisin trimers is regulated by large hook-shaped proteins composed of tandem HEAT repeats, known as HAWKs (HEAT repeat proteins associated with kleisins) [1].

The conundrum that complexes with such similar geometries appear to perform such dissimilar functions has been resolved by the realisation that cohesin also organises DNAs into chromatid-like structures, albeit during interphase and only upon ablation of a regulatory protein called WAPL [2] as well as naturally during meiotic prophase [3] or during V(D)J recombination when WAPL is downregulated in pro-B cells [4]. There is now considerable evidence that cohesin and condensin organise chromosomal DNAs during interphase and mitosis, respectively, by extruding DNA loops in a processive manner. Indeed, both exhibit such loop extrusion (LE) activity *in vitro* [5,6]. LE mediated by cohesin is halted or at least retarded at specific sequences bound by CTCF, and the processivity of the complex is reduced by WAPL which induces cohesin's dissociation from chromatin, albeit only infrequently every 10-20 min [7–9]. No such site-specific DNA binding proteins are known to regulate condensin. In both cases, chromatid formation is envisaged to arise from processive LE activity,

which organises DNA into a series of loops, each emanating from a central core containing the SMC-kleisin loop extruders [1].

Mammalian cells possess two types of condensin complexes: condensin I and II. Both complexes share the same SMC proteins, SMC2 and SMC4, which both contain 50 nm long anti-parallel coiled coils connecting a hinge domain at one end with an ATPase domain, formed from the N- and C-terminal extremities, at the other. Dimerisation via their hinges creates V-shaped SMC2/4 heterodimers whose ATPase heads are inter-connected by their kleisin subunits, NCAPH1 for condensin I and NCAPH2 for condensin II. These in turn recruit different HAWK regulatory subunits, NCAPD2 or D3 and NCAPG or G2 for condensin I and II respectively [10]. While condensin II remains in the nucleus during interphase and starts to organise chromosomal DNAs during prophase, condensin I only has access to the DNA after nuclear envelope break down [11–13]. Despite this difference, both accumulate along the longitudinal axes of metaphase chromosomes [13,14]. HiC data suggest that condensin I extrudes shorter loops that are nested within longer ones previously created by condensin II. Interactions between distant loops suggest that the loops created by condensin II may be organised radially around a coiled or solenoidal axis [15]. The ratio between condensin I and condensin II adjusts the coiling of chromosome axes, partly by altering the width of the central spiral and generating curled chromosomes [16].

An important factor in limiting the processivity of loop extrusion by cohesin is its release from chromatin. This process that depends on WAPL involves engagement of cohesin's ATPase heads [17] and dissociation of the N-terminal domain (NTD) of its SCC1 kleisin subunit from the coiled coil (neck) that emerges from SMC3's ATPase head domain [18]. Because a co-translational fusion of SCC1's NTD to the C-terminal domain of SMC3's ATPase blocks release, it has been proposed that it involves

passage of DNAs previously entrapped inside its SMC-kleisin ring through an exit gate created by dissociation of SCC1 from SMC3 [19,20]. Indeed, the kleisin NTDs appear to dissociate *in vitro* from engaged SMC2 and SMC4 heads [21,22] as well as those of SMC1 and SMC3 [19,23,24]. This observation raises the possibility that release via a kleisin-SMC exit gate might be a feature of chromosomal condensin complexes as well as cohesin. However, whether release of this nature occurs *in vivo* and whether it has an important function is not known.

Condensin II's activity and functions within the nuclei of interphase cells are poorly understood. While some studies have reported that it binds to chromatin during interphase [25], its depletion from post mitotic mouse liver cells has little or no effect on genome organisation or transcription [26]. Likewise, the notion that condensin II is activated as cells enter mitosis via kinase cascade involving CDK1 and PLK1 [27] also begs the question as to whether it has any significant role during interphase. However, an important clue that condensin II can in principle function during this stage of the cell cycle comes from the characterization of patients carrying a mutation of the *Mcph1* gene, which causes a reduction in the size of the cerebral cortex known as primary microcephaly (OMIM 608585) [28,29]. Cells from such patients have an increased number of prophase-like cells [30,31]. The prophase-like organisation of chromosomal DNA has since been shown to be mediated by condensin II [32,33], whose abnormal activity triggers premature condensation in G2 and late de-condensation in G1 [30,31,34].

MCPH1 is only found in metazoa. It contains three BRCT domains, one N-terminal and two C-terminal, separated by a disordered region. The diverse phenotypes of mutant cells have led to many different and often conflicting suggestions for its roles. Binding of MCPH1's C-terminal BRCT domains to phosphorylated histone H2AX [36] is thought to play a part in the DNA damage

response, while the premature chromosome condensation caused by mutations within its N-terminal BRCT has been attributed to this domain's defective association with the SWI/SNF nucleosome remodelling complex and SET1 [37]. MCPH1 is also thought to bind DNA and has been proposed to function in telomere maintenance, centriole organisation and CHK1 activation [38–42]. In contradiction to the finding that MCPH1 binds directly to condensin II, it is widely believed that the N-terminal ~200 residues of MCPH1 compete with condensin II for chromosomal binding [33], in other words, MCPH1 has been proposed to occupy loci required for condensin II's chromosomal activity.

Given the diversity and conflicting views of MCPH1's function, we have re-addressed its role in regulating chromosome structure by analysing the consequences of deleting its gene in mouse ES cells. We show that loss of MCPH1 induces a prophase-like organisation of chromatin during G1 and G2 but not during S phase, and that this depends on condensin II. Crucially, this phenotype, which is accompanied by condensin II's stable association with chromosomes, is unaffected by inhibiting CDK1, suggesting that MCPH1 does not inhibit chromosome condensation merely by delaying the CDK1 activation normally necessary for condensin II activity as previously suggested [40,41,43]. We demonstrate that MCPH1 instead regulates the organisation of chromosomal DNA through the binding of condensin II's NCAPG2 subunit by a conserved short linear motif (SLiM) situated within its central domain. Such binding does not *per se* explain how MCPH1 regulates condensin II and has little or no effect on its ATPase activity, at least *in vitro*. Presumably, other domains, for example its N-terminal BRCT, which is frequently mutated in human microcephaly patients, have an effector function, by interacting with other sites within the condensin II pentamer or recruit other cellular factors.

A clue to the role of MCPH1 is the resemblance between the stable association of condensin II with chromosomal DNA induced by MCPH1 ablation with the effect on cohesin of mutating *Wapl*, which binds to the cohesin HAWK equivalent to NCAPG2, namely STAG2, also using an FY SLiM. We therefore tested whether like WAPL, MCPH1 prevents condensin II from associating stably with DNA by opening the interface between NCAPH2's NTD with the neck of SMC2's ATPase domain. Remarkably, a translational fusion between SMC2's C-terminus and NCAPH2's N-terminus is not only functional in mouse oocytes but also resistant to the inhibition mediated by an excess of MCPH1 induced by mRNA micro-injection. This raises the possibility that like WAPL, MCPH1 acts by opening the interface between the kleisin's NTD and the neck of the SMC ATPase domain. Finally, we investigated the consequences of inducing the stable association with G2 chromosomes of both cohesin and condensin and found that the chromosomal axes created by cohesin upon mutating *Wapl* are turned into solenoids in cells deleted for both *Wapl* and *Mcph1*.

RESULTS

Mcph1 deletion induces chromosome condensation during interphase in embryonic stem cells.

Premature chromosome condensation is a key feature of cells isolated from patients carrying *Mcph1* mutations. To study this in greater detail, we used CRISPR/Cas9 to delete *Mcph1* in mouse E14 embryonic stem cells in which we had previously introduced a Halo-tag at the C-terminal end of NCAPH2 (NCAPH2-Halo) at its endogenous locus. Western blot using an anti-NCAPH2 antibody confirmed that all the NCAPH2 protein present in the cell is shifted to a higher molecular weight that

matches the size of the band detected by in-gel Halo-TMR fluorescence. The protein expression levels are identical to the untagged protein in control cells (Figure 1A). Deleting the second exon of *Mcph1* induces a frameshift between exon 1 and 3 and thereby complete inactivation of the gene. Western blot analysis of the targeted cells confirmed the lack of any MCPH1 protein (Figure 1A).

Immunofluorescence microscopy revealed that *Mcph1* deletion leads to a substantial increase in the fraction of cells with prophase like chromosomes (Figure 1B). FACS analysis of cells stained with propidium iodide to measure DNA content, H3PS10 specific antibodies to detect G2/M cells, and pulse labelled with EdU to identify S phase cells showed no overall change in cell cycle progression (Supplementary figure 1). Thus, *Mcph1* deletion caused little or no prophase arrest. Crucially, all EdU negative cells, whether they were in G1 (H3PS10 negative) or G2 (H3PS10 positive), contained prophase-like chromosomes (>100 cells counted) while few if any of the EdU positive S phase cells did so (Figure 1C and 3D). In wild type G1 and G2 cells, different centromeres and peri-centric regions cluster in chromocenters. This feature is abolished in the mutant cells, where every centromere occupies an individual location (Supplementary figure 2) and each chromosome is likewise individualised into prophase-like chromatids (Figure 1B). The localisation of NCAPH2 was analysed by labelling its Halo-tag with the fluorescent TMR ligand. In wild type, NCAPH2 has a diffuse nuclear distribution throughout most of the interphase, with no enrichment at any particular site. The protein starts to accumulate at centromeres during G2 and subsequently along the length of chromosomes from prophase until the end of telophase. Deletion of *Mcph1* caused NCAPH2 to associate with the prophase-like chromosomes in all G1 and G2 cells and become enriched at their individualised centromeres (Figure 1B).

MCPH1 restricts condensin II activity during G1 and G2.

The change in chromosome organisation caused by deletion of *Mcph1* is accompanied by a change in the localisation of condensin II. To address whether condensin II is causing the observed phenotype, we used a Halo-PROTAC ligand to specifically induce degradation of NCAPH2-Halo (Figure 1D). Because this completely reversed the re-organisation of chromosomal DNA caused by *Mcph1* deletion (Figure 1E), we conclude that altered regulation of condensin II is largely if not completely responsible. Unlike the centromere dispersion, chromosome condensation, and chromosome unpairing induced by loss of Slimb ubiquitin ligase or casein kinase 1 in *Drosophila* cells, which is accompanied and caused by an increase in the level of NCAPH2 [44,45], deletion of *Mcph1* in ES cells is accompanied by a modest but nevertheless significant reduction in NCAPH2 levels (Figure 1 A & D). The implication is that MCPH1 restricts the activity of individual condensin II complexes in G1 and G2 cells.

MCPH1 prevents condensin II's stable association with interphase chromatin.

Photobleaching studies with GFP tagged condensin II subunits has revealed that they are highly mobile during interphase, suggesting that they are rarely or only transiently associated with chromatin fibres [8]. FRAP of TMR labelled NCAPH2-Halo confirmed this as photobleached spots of Halo-TMR fluorescence recovered 95% of their fluorescence within 1 min (Figure 2). However, deletion of *Mcph1* caused a dramatic change in the dynamics, with fluorescence merely recovering to 28% of its starting level within 1 minute. After that, no further change occurred during the next 10 min (Figure 2), implying that *Mcph1* deletion causes 72% of condensin II complexes to

associate stably with chromatin in G1 or G2 cells, thereby altering chromatin compaction during interphase.

The chromosome re-organisation induced by *Mcph1* deletion does not depend on CDK1.

To check whether the premature formation of prophase-like chromatids when *Mcph1* deleted cells enter G2 might be caused by the precocious activation of CDK1, which activates condensin II as wild type cells enter prophase, we compared inhibitory phosphorylation of CDK1's Y15 residue and cyclin B1 localisation in wild type and mutant cells. Deletion of *Mcph1* neither reduced Y15 phosphorylation nor caused cyclin B1 to enter nuclei prematurely (Figure 3A and B). To address this issue more directly, namely whether CDK1 activity is required for condensin II's hyperactivity, we asked whether inhibition of the kinase would suppress the chromosomal re-organisation. Treatment of both wild type and *Mcph1* deleted cultures with the CDK1 inhibitor RO-3306 for seven hours caused most cells to accumulate in G2 with a 4C DNA content (Figure 3C). The DNA organisation of wild type cells resembled that of normal G2 cells, namely no chromatid-like structures were formed and centromeres were clustered in chromocenters (Figure 3D). In contrast, the chromosomal DNAs of all mutant cells were organized into prophase-like chromatids with individualised centromeres (Figure 3D). We conclude that the hyperactivity of condensin II in G2 *Mcph1* deleted cells is independent of CDK1, suggesting that MCPH1 regulates condensin II directly.

***Mcph1* deletion induces chromosomal compaction and alters inter-chromosomal interactions**

In situ Hi-C libraries were generated for wild-type mouse E14 and *Mcph1* deleted cells. In wild-type cells, chromosomal p-termini have enhanced contact frequencies with one another, as do q-termini. In contrast, p-termini are less likely to contact q-termini (Figure 4A). This is consistent with the presence of chromocenters within which p-termini co-localize with each other and likewise q-termini with each other. Because mouse chromosomes are telocentric, with centromeres located at their p-termini, the HiC maps confirm that centromeres co-localize with one another as do telomeres.

Strikingly, the enhanced spatial proximity between chromosomal p-termini (resp., q-termini) is lost in the absence of MCPH1 (Figure 4B and C), consistent with the disappearance of chromocenters as observed by microscopy. Deletion of *Mcph1* also results in an enhancement in the frequency of long-range, intra-chromosomal contacts (Figure 4D, E and F) and enhances the frequency of inter-compartment (A to B) contacts as compared to intra-compartment contacts (A to A and B to B) (Supplementary figure 3A and B). This finding is consistent with the compaction of individual chromosomes upon loss of MCPH1.

The HiC maps did not reveal loci moving from one compartment to the other nor any major changes in loops or contact domains (Supplementary figure 3C).

Recombinant MCPH1 forms a stable complex with condensin II.

Our results suggest that MCPH1 directly represses condensin II activity, possibly via a direct interaction. Previous *in vitro* work suggested that MCPH1 binds condensin II via two interfaces. One interface between the N-terminal 195 residues of MCPH1 and NCAPD3 and a second binding site between a highly conserved central domain of MCPH1 (381-435) and NCAPG2 (Figure 5A and B) [33]. To confirm a direct interaction between MCPH1 and condensin II, full length human MCPH1 and condensin II were

expressed in insect cells and separately purified. While full-length MCPH1 was largely insoluble, we purified sufficient strep-tagged full-length MCPH1 to confirm that it could pull-down pentameric condensin II complex (Figure 5C). To localise the binding site, we expressed and purified N-terminal His-MBP-tagged truncations of MCPH1 in *E. coli*: MBP-MCPH1$_{1\text{-}435}$, MBP-MCPH1$_{1\text{-}195}$, MBP-MCPH1$_{196\text{-}435}$ and MBP-MCPH1$_{348\text{-}469}$ (Figure 5A). We found that strep-tagged condensin II could only pull-down MCPH1 constructs that included the central domain (Figure 5D). MCPH1 binding was specific to condensin II, as condensin I-strep was unable to pull down any MCPH1 constructs (Supplementary figure 4A).

We then tested whether tetrameric condensin II, lacking either NCAPD3 or NCAPG2, could bind MCPH1$_{1\text{-}435}$ using pull-down assays. To exclude the MBP tag interfering with the interaction at the N-terminus of MCPH1, we moved the tag to the C-terminus. We found that removing NCAPG2 greatly reduced MCPH1$_{1\text{-}435}$ MBP pull-down, while removing NCAPD3 had no effect (Figure 5E), suggesting that the binding was mediated by the central domain of MCPH1 to NCAPG2. Further analysis with analytical size exclusion chromatography demonstrated that MBP-MCPH1$_{196\text{-}435}$ and condensin II co-eluted in one peak, separated from the void volume, suggesting they form a stable, soluble complex (Supplementary figure 4B).

MCPH1 binds condensin II via a short linear motif.

To address which part of MCPH1's central domain is necessary for binding condensin II, we analysed the sequence of MCPH1 using the ConSurf server [46,47] to identify conserved sequences. Between residues 381-435 of human MCPH1, the 410-424 interval stands out as a highly conserved patch within a region that is otherwise poorly conserved (Figure 5B and Supplementary figure 4C). Despite its conservation, the

sequences are predicted to be disordered, suggesting that it could be a short linear motif (SLiM) that binds to condensin II. To test this, we performed fluorescence polarisation binding assays with a 5-FAM labelled MCPH1 peptide spanning residues 407-424 and found that it bound to condensin II, with a fit Kd of 0.64 ± 0.12 μM (mean ± SEM) (Figure 5F). As expected, no binding was detected to a tetrameric version of condensin II lacking NCAPG2.

SLiMs are frequently regulated by post-translation modification [48] and proteomic analysis of mitotic cells previously found that MCPH1 can be phosphorylated within the central motif at S417 [49], with S417/P418 forming a potential CDK consensus site [50]. We therefore used a fluorescence polarisation competition assay to test the effect of phosphorylating S417. In these assays, the concentration of condensin II and 5-FAM-MCPH1$_{407-424}$ is fixed and unlabelled peptides of either wild-type or S417 phosphorylated MCPH1$_{407-424}$ are added at increasing concentrations. While the wild-type MCPH1$_{407-424}$ readily competed with 5-FAM-MCPH1$_{407-424}$, resulting in a fit competition K_D of 5.3 ± 1.0 μM, phosphorylation at S417 reduced the affinity ~10 fold to 53 ± 8 μM (Figure 5G). This suggests that CDK1 phosphorylation of MCPH1 may reduce its interaction with condensin II, an effect that might have an important role in initiating chromosome condensation during prophase.

MCPH1 central domain is essential for its interaction with condensin II and its regulation *in vivo.*

To address whether this central motif is necessary for binding and regulating condensin II *in vivo*, we created an E14 cell line in which both copies of the *Ncaph2* gene is tagged at its C-terminus with GFP. Western blotting revealed MCPH1 in immunoprecipitates generated using antibodies against GFP, and only in GFP-tagged

cells expressing wild-type MCPH1 (Figure 6A). Because the MCPH1-specific antibody was raised against the central domain, we used a cell line in which both copies of *Mcph1* and *Ncaph2* were tagged with GFP and Halo respectively to test the role of the central domain motif and then created a variant (*Mcph1*$^{\Delta CenGFP/\Delta CenGFP}$) lacking 15 residues containing the motif (S_{400}SYEDYFSPDNLKER$_{414}$). Western blotting confirmed that *Mcph1*$^{GFP/GFP}$ cells and *Mcph1*$^{\Delta CenGFP/\Delta CenGFP}$ were expressed at similar levels (Figure 6C). The slightly increased mobility of *Mcph1*$^{\Delta CenGFP/\Delta CenGFP}$ and its failure to be detected by the MCPH1-specific antibody confirmed deletion of the central domain motif (Figure 6B). Because TMR labelled NCAPH2-Halo was detected in GFP immunoprecipitates from *Mcph1*$^{GFP/GFP}$ but not *Mcph1*$^{\Delta CenGFP/\Delta CenGFP}$ cells (Figure 6C), we conclude that MCPH1's central domain is essential for its stable interaction with condensin II *in vivo*.

Immunofluorescence revealed that MCPH1 and MCPH1$^{\Delta Cen}$-GFP proteins show the same localisation within cells. They are both exclusively nuclear and enriched in small clusters that colocalise with sites of DNA damage marked by γH2aX DNA (Figure 6D), as previously reported [51]. The significance of this association is unclear as *Mcph1* deletion has no effect on the level of γH2aX (Supplementary figure 1D). Crucially, the chromosomes of *Mcph1*$^{\Delta CenGFP/\Delta CenGFP}$ but not *Mcph1*$^{GFP/GFP}$ G1 and G2 cells adopted the prophase-like appearance characteristic of *Mcph1* deleted cells (Figure 6E). Therefore, we conclude that MCPH1's central domain SLiM is essential for inhibiting condensin II during interphase and inhibiting premature condensin-mediated chromatin condensation.

MCPH1 does not alter condensin II ATPase activity or DNA binding *in vitro.*

To address whether MCPH1 affects condensin II's activity *in vitro*, purified the condensin II- MCPH1$_{1-435}$ complex using size exclusion chromatography and measured its ATPase activity. The condensin II-MCPH1$_{1-435}$ complex possessed a similar activity to that of condensin II alone but its stimulation by DNA was modestly lower (Figure 7A). To ensure that the ATPase activity measured in these assays was genuinely due to condensin II, we also purified a condensin II-MCPH1$_{1-435}$ complex deficient in ATP binding (Q-loop mutation, SMC2 Q147L, SMC4 Q229L). As expected, this mutation effectively eliminated ATPase hydrolysis (Figure 7A).

Previous work has suggested that full length MCPH1 binds to DNA and chromatin [33,42] so we tested whether MBP-MCPH1$_{1-435}$ and MBP-MCPH1$_{196-435}$ are able to bind to a 50 bp sequence of dsDNA using electrophoretic mobility shift assay (EMSA). Both MCPH1$_{1-435}$-MBP and MCPH1$_{196-435}$-MBP were able to induce a shift, however higher concentrations of MCPH1$_{196-435}$ MBP were required for a complete shift in the free DNA band, suggesting MCPH1$_{1-195}$ MBP could have a role in DNA binding (Figure 7B). We then examined if MCPH1 affected condensin II DNA binding, by performing condensin II EMSAs in the presence or absence of MCPH1$_{1-435}$-MBP. The distinct MCPH1$_{1-435}$-MBP shifted band disappeared with increasing concentrations of condensin II, and there was an upward shift in the condensin II bands in the presence of MCPH1$_{1-435}$-MBP relative to the MBP condensin II control, suggesting MCPH1 was binding with condensin II (Figure 7C). We then performed condensin II EMSAs in the presence or absence of 1μM 5-FAM-MCPH1$_{407-424}$ peptide. 5-FAM signal was present with condensin II shifted DNA band demonstrating that the MCPH1 peptide was sufficient to mediate comigration of MCPH1 with condensin II (Figure 7D). Additionally, the presence of the 5-FAM-MCPH1$_{407-424}$ peptide did not affect condensin II DNA binding. Collectively, this indicates that *in vitro*, using purified

proteins, condensin II can bind MCPH1 and DNA simultaneously. Finally, these results suggest that the inhibitory effect of MCPH1 on condensin II loading observed *in vivo* involves a feature absent from the *in vitro* DNA binding assay.

MCPH1 overexpression inhibits the loading of condensin II on mouse meiotic chromosomes.

Our results show that MCPH1 plays a crucial role in chromosome organisation during interphase by inhibiting condensin II's activity in mitotic cells. We next extended our analysis of MCPH1 to meiotic cells by testing the effect of increased MCPH1 expression during the first meiotic division of mouse oocytes. To image the chromosomes, oocytes were injected with *in vitro* transcribed mRNA coding for H2B-mCherry to illuminate the chromosomes in magenta (Figure 8A). As previously described [52], after the germinal vesicle breakdown (GVBD), bivalent chromosomes form a ball (3.3 h) before congressing to a metaphase plate (7.4 h). Cleavage of cohesin by separase along chromosome arms then converts each bivalent into a pair of dyads that segregate highly synchronously to opposite poles of the cells during anaphase I (10 h), which is followed by extrusion of the first polar body (Figure 8B, control).

Co-injection with *M. musculus* MCPH1 mRNAs (Figure 8B, +MCPH1) had little effect on the chromosome congression until metaphase. However, it caused chromosomes to unravel soon after the onset of anaphase, presumably because chromosomes are not stiff enough to resist to the pulling forces of the spindle, and this was accompanied by a catastrophic failure to disjoin the chromosome arms of dyads to opposite poles (Figure 8B, +MCPH1, 16 h). The lack of chromosome rigidity and

the unravelling of the chromatin in response to traction by the spindle are reminiscent of the phenotype caused by depletion of NCAPH2 [52].

To address whether MCPH1 overexpression inhibits the association of condensin II with chromosomes, we rescued mouse oocytes deleted for *Ncaph2* (*Ncaph2*$^{Lox/Lox}$*; ZP3*^{TgCre}) by injecting an mRNA coding for NCAPH2-GFP as previously described [52]. These oocytes were also injected with mRNA encoding MAD2 to arrest them in meiosis I and H2B-mCherry to image and quantify the amount of chromosomal NCAPH2-GFP (Figure 8C). This revealed that the injection of MCPH1 mRNAs greatly reduced association of condensin II with chromosomes during metaphase I (Figure 8D and E). To see if MCPH1 can also release condensin II previously associated with chromosomes, we injected MCPH1 mRNA into meiosis I arrested oocytes. However, this induced a much milder reduction within the first two hours (not shown), suggesting that MCPH1 prevents the initial loading of condensin II on chromosomes but has little effect on complexes already stably associated with them.

The N-terminal BRCT domain of MCPH1 was previously shown to have an essential role in regulating chromosome condensation both *in vitro* and *in vivo* [33]. Consistent with this, deletion of the N-terminal 200 amino acids of MCPH1 abolishes its inhibitory effect in mouse oocytes (Figure 8D). It has also been claimed that the N-terminal domain of MCPH1 can on its own inhibit condensin II by competing for its binding sites on chromosomal DNA [33]. However, we were unable to detect any impact of over-expressing only the NTD of MCPH1 (not shown).

Fusion of SMC2 to NCAPH2 is resistant to MCPH1 inhibitory effect.

The effects of MCPH1 on condensin II resemble those of WAPL on cohesin, which is thought to act by dissociating the NTD of its kleisin from the neck of SMC3's

ATPase domain [18,19,53]. A key finding in this regard is that the fusion of the C-terminus of SMC3 to the N-terminus of SCC1 causes cohesin to resist WAPL. To address whether fusion of this nature has similar effect on condensin II, we created a cDNA encoding a protein in which the C-terminus of SMC2 and the N-terminus of NCAPH2 are connected by a 57 amino acid linker containing three TEV protease cleavage sites. A GFP tag was introduced at the C-terminal end of NCAPH2 to image the protein (Figure 9A). Importantly, mRNAs encoding this fusion fully rescued the meiosis I chromosome segregation defects of oocytes deleted for *Ncaph2*. Furthermore, GFP fluorescence associated with the fusion protein was detected along the chromosome axes of bivalent chromosomes, a distribution that is similar if not identical to that of wild-type NCAPH2. Remarkably, co-injection of MCPH1 mRNAs had no adverse effect on this activity, unlike controls in which MCPH1 mRNAs were co-injected with NCAPH2-GFP mRNAs (Figure 9B and C). Likewise, MCPH1 prevented association of NCAPH2-GFP with chromosomes but not that of the SMC2-NCAPH2-GFP fusion (Figure 9C).

A caveat to this experiment is that the resistance to MCPH1 of the SMC2-NCAPH2-GFP fusion could be due to the linker sequences associated with the N- and C-termini of NCAPH2 and SMC2 respectively rather than their stable inter-connection *per se*. If the latter were the case, cleavage of the linker using TEV protease should restore sensitivity to MCPH1. We therefore repeated the rescue experiment but, in this case co-injected mRNA encoding TEV protease (Figure 9D). Quantification of the chromosomal GFP fluorescence showed that the fusion's resistance to MCPH1 activity is abolished by the TEV (Figure 9E and F), which is consistent with the notion that resistance arises from connecting the interface between SMC2 and NCAPH2.

Mcph1 deletion induces the coiling of cohesin vermicelli.

Our results suggest that condensin II's association with chromosomal DNA might be regulated by MCPH1 through a mechanism that resembles that of cohesin by WAPL. By inducing cohesin's dissociation from chromatin, albeit only rarely approximately every 15 min., WAPL merely moderates the processivity of loop extrusion mediated by cohesin. MCPH1 has a more drastic effect, preventing most condensin II complexes from ever associating stably with chromatin. The entire architecture of interphase chromatin therefore depends on these two key regulatory factors. Though condensin II is presumed like cohesin to act as a DNA loop extruder, the deregulation of cohesin and condensin II induces different chromosomal morphologies. *Wapl* deletion enables cohesin to form thread-like structures and to accumulate along their longitudinal axes, creating so called vermicelli. In contrast, *Mcph1* deletion enables condensin II to produce soft spherical or "gumball" chromosomes and to associate stably throughout chromosomal DNA, albeit at high levels at centromeres. Strangely, condensin II does not form or accumulate along the sort of axes observed when wild type cells enter mitosis. Thus, the activities of condensin II and cohesin unleashed by *Mcph1* and *Wapl* deletion respectively produce DNA loops with very different arrangements. We therefore set out to address two questions. First, is this difference intrinsic to differences in the behaviour of cohesin and condensin II or merely due to differences in the type of cell used, namely mouse fibroblasts and ES cells? Assuming that it is in fact, the former, what happens when both factors are deregulated simultaneously? To this end, we altered the *Mcph1* and *Wapl* genes in E14 cells in which SCC1 is tagged with Halo and NCAPH2 with GFP. Because *Wapl* deletion is lethal, we generated a tamoxifen-inducible deletion allele, which enabled us to compare chromosomal DNA morphology as well as localisation of SCC1-Halo and

NCAPH2-GFP in four different conditions: Wild type, *ΔWapl*, *ΔMcph1* and the double mutation *ΔWapl, ΔMcph1* (Supplementary figure 5).

In wild-type cells, SCC1-Halo accumulates throughout nuclei and their genomes during interphase and apart from centromeres, is largely removed from chromosomes through the action of WAPL in M phase. Condensin II's distribution resembles that of cohesin throughout most of interphase (Figure 2 and [8]). Condensin II accumulates around centromeres during G2 and along the chromatid axes created through its activity during prophase (Figure 10, WT).

As previously reported for fibroblasts, *Wapl* deletion in E14 cells causes cohesin to create chromatid-like structures, especially during G2, and to accumulate along their longitudinal axes [2]. Because the majority of SCC1 remains on chromosomes during mitosis, most is cleaved by separase during anaphase and daughter cells inherit considerably less cohesin than normal. As a consequence, axial cohesin vermicelli are rarely if ever observed during G1, especially as this cell cycle phase is very short in ES cells. Pronounced vermicelli are only observed in G2. As expected, *Wapl* deletion neither alters condensin II's distribution during interphase nor hinders its accumulation along chromatid axes during mitosis. Despite cohesin's persistence on mitotic chromosomes and the participation of a large fraction in sister chromatid cohesion, condensin II still manages to localise to and help create the axes of individual chromatids, between which run inter-chromatid axes coated in cohesin (Figure 10A and B, Δ*Wapl*). There are presumably two pools of chromosomal cohesin in post-replicative *Wapl* deleted cells, one involved in cohesion and a second engaged in the loop extrusion responsible for the formation of vermicelli. The former clearly persists and accumulates along the inter-chromatid axis when loop extrusion mediated by condensin I and II individualise chromatids, but the fate of the latter is unclear.

Deletion of *Mcph1* had little effect on cohesin's distribution. Despite the formation of gumball chromosomes during G1 and G2, cohesin remains uniformly associated with chromatin and does not form vermicelli. As in wild type cells, most dissociates from chromosome arms when cells enter mitosis and little can be detected along the inter-chromatid axes connecting the two condensin II axes of individualised chromatids (Figure 10, Δ*Mcph1*).

Deletion of both *Wapl* and *Mcph1* had a dramatic effect. The cohesin vermicelli caused by the lack of WAPL in G2 cells adopt a coiled configuration upon the simultaneous deletion of *Mcph1*. This coiling increases during prophase. By the time cells reach metaphase, the coiling leads to the formation of chromosomes that have the shape of a spring (or solenoid), a configuration that is visible with SCC1-Halo, NCAPH2-GFP and DNA staining (DAPI) (Figure 10, Δ*Wapl,* Δ*Mcph1*). Moreover, the two distinct axes of condensin II associated with each chromatid remain intermingled in the double mutant.

To analyse the axial organisation of these chromosomes in greater detail, we used super-resolution three-dimensional structured illumination microscopy (3D-SIM) to compare the distribution of SCC1-Halo in *Wapl* deleted and double mutant cells. Unfortunately, fluorescence due to NCAPH2-GFP was insufficient to reveal reliable images using this technique. Analysis of G2 cells revealed that a modest coiling of cohesin axes surrounded by DNA loops in *Wapl* single mutants is greatly accentuated in double-mutant cells, with a pronounced increase in the radii of coils (Figure 11 and Supplementary video 1). In metaphase cells, the cohesin axes that seem to have a spring-like appearance in confocal microscopy are revealed to have a much more complicated organisation, being composed of twisted segments that regularly change handedness. It is noticeable that the formation of chromosomes with this morphology

525 is not simply due to the combined activity/presence of cohesin and condensin II during
526 mitosis, which also occurs in *Wapl* single mutants. It only arises when both cohesin
527 and condensin were stably associated with chromatin during G2.

528 We conclude that combining the abnormal activity of condensin II unmasked by
529 deleting *Mcph1* with that of cohesin unmasked by deleting *Wapl* leads to a major
530 transformation of chromosome structure when cells enter G2, that is associated with
531 coiling of the entire axis of the chromosome. Interestingly, this coiling does not have a
532 handedness that persists throughout the chromosome in metaphase. Instead, the
533 chromosome appears divided into segments whose axes are coiled with alternating
534 handedness.

535

536 **DISCUSSION**

537 Despite accumulation within interphase nuclei, condensin II associates with chromatin
538 only fleetingly if at all and exerts little or no effect on chromosome topology during this
539 phase of the cell cycle. It normally only associates stably with chromosomal DNA and
540 organises it into a series of loops when cells enter M phase. The restriction of
541 condensin II's activity to M phase was previously attributed to its phosphorylation by
542 CDK1 [27,40,41,43]. Our finding that in the absence of MCPH1, condensin II is capable of
543 transforming the topology of chromosomal DNA in cells arrested in G2 using a CDK1
544 inhibitor implies that condensin II is capable of substantial activity in the absence of
545 CDK1-mediated phosphorylation normally associated with M phase. In other words, it
546 is MCPH1 that prevents condensin II's association with chromosomes during G2 not
547 the lack of CDK1 phosphorylation.

548 Our observation that phosphorylation of a CDK1 consensus sequence
549 abolishes association between a conserved and essential SLiM within MCPH1's

central domain and condensin II's NCAPG2 subunit raises the possibility that CDK1 exerts at least part of its effect by preventing MCPH1's association with condensin II. Our conclusion that the SLiM within MCPH1's central domain is essential for its inhibitory activity contradicts the claim that it is not necessary, an inconsistency that we attribute to the fact that previous studies tested the function of over-expressed MCPH1 alleles [33,54].

Our findings as well as those of others [30,31,35] show that MCPH1 is responsible for inhibiting condensin II during G1 as well as G2 phase. Thus, in the absence of MCPH1, condensin II organises chromosomal DNAs into chromatid-like structures during G1 and G2 but strikingly not during S phase when some other (MCPH1-independent) mechanism prevents it from associating stably with chromatin.

MCPH1's inhibition of condensin II depends on its N-terminal BRCT domain in addition to its central SLiM. Indeed, most of *Mcph1* mutations identified in microcephaly patients affect the BRCT domain, which possibly interacts with some other part of condensin II once MCPH1 has been recruited via its SLiM. However, the function of this domain remains mysterious.

How does MCPH1 inhibit condensin II? An important clue stemmed from the numerous similarities between MCPH1 and WAPL, a protein that facilitates cohesin's release from chromatin [1]. WAPL binds to STAG, the cohesin subunit equivalent to NCAPG2, using a SLiM and its inactivation leads to cohesin's stable association with chromatin [2,7,55]. Cohesin release mediated by WAPL involves dissociation of the NTD of cohesin's SCC1 kleisin subunit from the coiled coil that emerges from SMC3's ATPase head, known as its neck [18,19,53]. It is currently thought that kleisin-neck dissociation takes place, albeit rarely, upon engagement of cohesin's SMC1 and SMC3 ATPase heads in the presence of ATP when SMC3 is unacetylated and in the

absence of SCC2 [18,19,56,57]. Crucially, the fusion of SMC3's C-terminus to SCC1's N-terminus completely blocks WAPL from triggering cohesin's release from chromatin [19,53]. It could do so either by creating a barrier to the passage of DNA through an opened kleisin-neck interface, i.e. by blocking the exit of DNAs previously entrapped within cohesin rings, or merely by hindering kleisin-neck dissociation, which has some other poorly understood function necessary for release.

Our finding that an analogous fusion, between the C-terminus of SMC2 and the N-terminus of NCAPH2, prevents the release of condensin II from meiosis I chromosomes in oocytes upon over-expression of MCPH1 suggests that MCPH1 prevents condensin II's association with chromatin by a mechanism that is similar to cohesin's release by WAPL. It has been reported that engagement of SMC2 and SMC4 heads triggered by ATP binding induces the release of the NTD of the kleisin from SMC2's neck [21,58], raising the possibility that MCPH1 blocks condensin II's stable association with chromatin by facilitating such a process. Irrespective of the actual mechanics, which remains poorly understood, our observations emphasise that MCPH1 blocks condensin II's association with chromosomes using a mechanism similar to that that employed by WAPL to cause cohesin release.

Despite these striking similarities, the mode of action of these two proteins may differ in an important respect. Though WAPL alters cohesin's residence time on chromatin exclusively by facilitating release, our finding that over-expression of MCPH1 in oocytes prevents *de novo* association of condensin II but does not remove complexes previously associated with chromosomes raises the possibility that MCPH1 acts predominantly by aborting *de novo* loading.

Recent advances have shown that both human condensin and cohesin complexes extrude DNA loops [5,59–61], and cryo-electron microscopy structures of yeast

condensin, and yeast and human cohesin are starting to provide insight into how these complexes engage with DNA [58,62–64]. In the case of cohesin, it has been suggested that an early step is the clamping of DNA on top of SMC1 and SMC3 ATPase domains that have engaged with each other in the presence of ATP. Clamping in this manner requires cohesin's SCC2 HAWK protein, which is equivalent to condensin II's NCAPD3. SCC2 is necessary to prevent cohesin's release from chromatin and may perform this function by preventing dissociation of its kleisin subunit from SMC3's neck [57,62]. If NCAPD3 had a similar role, then MCPH1 could conceivably block condensin II's association with chromatin by interfering with NCAPD3's ability to block the release of NCAPH2 from SMC2.

One of the earliest insights into the cell division cycle was that one of the main constituents of the nucleus undergoes a dramatic morphological transformation shortly before division, namely the transformation of an apparently amorphous mass of chromatin into thread-like structures now known as chromosomes, each composed of a pair of chromatids joined together. It is now recognised that this transformation is brought about by condensins I and II which act by extruding DNA loops. It is also recognised that interphase chromosomal DNA is not in fact amorphous but instead characterised by a complex and dynamic network of interactions known as topologically associated domains or TADs, which are created by cohesin that like condensin is a DNA loop extruder, albeit one that is active during interphase and blocked by the site specific DNA binding protein CTCF [55,65].

There are two reasons why DNAs are not organised into thread-like chromatids during interphase. By causing cohesin release, WAPL prevents loop extrusion by cohesin going to completion while MCPH1 prevents condensin II associating with DNA stably and thereby extruding loops. Crucially, inactivation of either protein leads to the

formation of chromatid-like structures during interphase, albeit by different loop extruders and with different actual morphologies. Interestingly, depletion of both proteins simultaneously leads to a major transformation of chromosome structure as cells enter mitosis, which is associated with coiling of the entire axis of the chromosome. Understanding how and why this comes about through the unregulated activities of cohesin and condensin II may help reveal further insight into how loop extrusion creates chromosomes.

Glossary:

HAWK, HEAT repeat protein associated with the kleisin

LE, loop extrusion

PLC, prophase like cells

SLiM, short linear motif

TADs, topologically associating domains

Cryo EM, cryo electron microscopy

AFM, atomic force microscopy

GVBD, germinal vesicle break down

Acknowledgements

We thank N. Halidi and C. Monico for technical assistance, M. Inês Baptista for her advice on cloning the STOP cassette, A. Szczurek for his help in fluorescence quantification, S. Mahara for FACS analysis, M. Ranes and S. Guettler for the MBP vector and N. Davey for SLiM conversations.

Funding

This work was supported by the Wellcome Trust (Grant Ref 107935/Z/15/Z), ERC grant (Proposal No 294401) and Cancer Research UK (26747). Imaging was performed at the Micron Oxford Advanced Bioimaging Unit funded by a Wellcome Trust Strategic Award (091911 and 107457/Z/15/Z). Funding for MSS was provided by the Paul and Daisy Soros Foundation.

Author contribution

MH design, performed the experiments, wrote the manuscript and coordinated the project. EC designed, performed all the *in vitro* biochemistry experiments and wrote the manuscript. JG provided advice for the manipulation of oocytes. LS acquired and analysed the SIM data. APA performed the Hi-C experiments. ELA supervised HiC experiments and wrote the corresponding section. MSS and DW processed and analyzed the Hi-C data. AV supervised the project and wrote the manuscript. KN supervised the project and wrote the manuscript.

Competing financial interests

The authors declare no competing financial interests.

FIGURE LEGENDS

Figure 1. *The deletion of Mcph1 in E14 cells induces condensin II-dependent chromosome condensation in both G1 and G2 phases of the cell cycle*. **(A)** In gel TMR-Halo detection and Western blot analysis of E14 cells wild type, *Ncaph2*$^{Halo/Halo}$ and *Ncaph2*$^{Halo/Halo}$ *Mcph1*$^{\Delta/\Delta}$. TMR signal detects NCAPH2-Halo tagged. The anti-NCAPH2 antibody shows that all the NCAPH2 protein expressed is fused to the Halo-tag and that the expression levels are similar to wild type but reduced after *Mcph1* deletion. The anti-SMC2 detection shows similar levels of condensin in the three cell lines. **(B)** Immunofluorescence analysis of Histone H3 phosphorylated on serine 10 (green) combined with TMR detection of NCAPH2-Halo (Red) in *Mcph1*$^{wt/wt}$ and *Mcph1*$^{\Delta/\Delta}$ cells. The DNA organization was analysed using Hoechst. **(C)** EdU incorporation in *Mcph1*$^{wt/wt}$ or *Mcph1*$^{\Delta/\Delta}$ cells. **(D)** Western blot analysis of Halo-PROTAC induced NCAPH2-Halo degradation in wild-type, *Ncaph2*$^{Halo/Halo}$ *Mcph1*$^{wt/wt}$ and *Ncaph2*$^{Halo/Halo}$ *Mcph1*$^{\Delta/\Delta}$ cells using an anti-NCAPH2 antibody. Anti-SCC1 was used as a loading control. **(E)** Immunofluorescence analysis of the chromosome decompaction induced by 16 h treatment of *Mcph1*$^{\Delta/\Delta}$ cells with Halo-PROTAC. Immunofluorescence analysis of Histone H3 phosphorylated on serine 10 (green) was used to compare similar cell cycle stages. Scale bar, 5 μm.

Figure 2. *Mcph1 deletion induces the stable binding of condensin II to the condensed chromosomes in interphase.* FRAP analysis of NCAPH2-Halo turn-over on chromatin in *Mcph1*$^{wt/wt}$ **(A)** and *Mcph1*$^{\Delta/\Delta}$ cells **(B)**. Top row: NCAPH2-Halo signal pre-bleach, post bleach and after 70 sec recovery. The region bleached correspond to the white circle. Scale bar, 5 μm. **(C)** Quantification of the fluorescence recovery after photobleaching over a 10 min post-bleach period. (Average of three experiments, total

695 number of cells analysed: WT 28 cells, *Mcph1*$^{\Delta/\Delta}$ 30 cells, standard deviation is
696 represented for every time point)
697
698 **Figure 3.** *CDK1 activity is not required for the condensation phenotype induced by*
699 *Mcph1 deletion.* **(A)** Western blot analysis of CDK1 phosphorylation on tyrosine 15 in
700 wild type cells compared to *Mcph1* deleted cells. Wild-type protein extracts were
701 treated by λ phosphatase as a control of antibody specificity. An anti-CDK1 protein
702 was used as a loading control. **(B)** Immunolocalisation of Cyclin B in *Mcph1* deleted
703 cells. **(C)** CDK1 activity was inhibited by incubating wild-type or *Mcph1* deleted cells
704 to RO-3306 for 7 h. The cell cycle profile was analysed by FACS for both wild-type
705 and *Mcph1* deleted cells without treatment or after 7 h incubation with 9 μM R0-3306.
706 **(D)** All the G2 cells in *Mcph1* deleted cells present the condensed phenotype after
707 CDK1 inhibition. Scale bar, 5 μm.
708
709 **Figure 4**. *Mcph1 deletion causes chromosome compaction and loss of*
710 *chromocenters*. **(A)** Representative subset of interactions between chromosomes 1-7
711 for wild-type and *Mcph1* deletion maps (wild-type below diagonal) shows loss of
712 chromocenters in the *Mcph1* deletion maps. **(B)** Log fold change for *Mcph1* deletion
713 over wild-type for chromosomes 1-7. **(C)** Log fold enrichment of the *Mcph1* deletion
714 map over wild-type map for the aggregated inter-chromosomal matrix. **(D)** Balanced
715 KR-normalized Hi-C Maps for wild-type and *Mcph1* deletion maps for the
716 intrachromosomal region of chromosome 1 (wild-type below diagonal). Increased
717 interactions between distant loci in the intrachromosomal *Mcph1* deletion maps is
718 seen. Color scale threshold is at the average value of each respective Hi-C map. **(E)**
719 Intrachromosomal contact probability for all chromosomes shows increased long-

720 range interactions and diminished contact drop-off for *Mcph1* deletion. **(F)** Average
721 intrachromosomal contact frequency for all chromosomes shows increased long-
722 range interactions with *Mcph1* deletion.
723
724 **Figure 5.** *Human condensin II interaction with MCPH1*. **(A)** Domain structure of
725 MCPH1 and MBP fusion constructs that were expressed in *E. coli* and used in binding
726 assays. BRCT domains are indicated in green and the central domain in yellow. **(B)**
727 Conservation analysis of the MCPH1 central domain with the ConSurf server. **(C)**
728 Strep tag pull-down indicating full length MCPH1 binds condensin II. Full length
729 MCPH1 and condensin II were expressed in insect cells and separately purified,
730 before being mixed on strep-tactin sepharose. Samples of input and resin after run on
731 SDS page and visualised with silver stain. **(D)** Strep-tag pull-down assay indicating
732 strep tagged condensin II pulls down MBP-MCPH1 constructs that contain the central
733 domain, but not MBP-MCPH1$_{1\text{-}195}$ or MBP alone. SDS page gel visualised with
734 Coomassie stain. **(E)** Strep pull-down assay showing strep-tagged pentameric
735 condensin II or tetrameric condensin II lacking NCAPD3 can pull down MBP-MCPH1$_{1\text{-}$
736 $435}$, while tetrameric condensin lacking NCAPG2 does not pull down MCPH1. The
737 lower panel shows a western blot performed using strep-resin samples, blotted using
738 an anti-NCAPD3 antibody. **(F)** Fluorescence polarization binding assay using 5-FAM
739 labelled MCPH1$_{407\text{-}424}$ peptide and increasing concentration of either pentameric
740 condensin or tetrameric condensin II lacking MCPH1 binding subunit NCAPG2
741 (CIIΔG2). **(G)** Peptide competition assay using a fixed concentration of 5-FAM labelled
742 MCPH1$_{407\text{-}424}$ and condensin II with an increasing amount of MCPH1$_{407\text{-}424}$ wild-type
743 or phosphorylated at serine 417. All error bars indicate standard deviation from three
744 replicates.

Figure 6. *MCPH1 interaction with condensin II is essential to prevent interphasic chromosome condensation.* **(A)** Co-immunoprecipitation of MCPH1 with NCAPH2-GFP. Nuclear extracts were prepared from wild type, *Ncaph2*$^{GFP/GFP}$ and *Ncaph2*$^{GFP/GFP}$ *Mcph1*$^{\Delta/\Delta}$ cells. Immunoprecipitation was performed using GFP-trap agarose beads and analysed by western blot using an anti-MCPH1 antibody (IP-GFP). 5% of the lysate used for IP was loaded as INPUT control. Anti-Lamin B1 antibody was used as a loading control. **(B)** Deletion of the central domain of MCPH1. To address if the central domain of MCPH1 is necessary to mediate the interaction with condensin II, we first introduced a GFP-tag at the C-terminal end of MCPH1 in *Ncaph2*$^{Halo/Halo}$ cells as the antibody against the protein was raised against the central domain. Then a second targeting was done to delete the central domain. As a result, the western blot represented in panel B using anti-MCPH1 antibody detects the wild-type protein or the GFP-tagged protein, homozygous *Mcph1*$^{GFP/GFP}$ but does not detect anything after deletion of the central domain. Using anti-GFP antibody reveals that the protein deleted for the central domain is present in the cell at similar levels as the wild-type GFP-tagged protein. A slight decrease in size is observed due to the deletion of the central domain. Anti-Lamin B1 antibody was used as a loading control. **(C)** Co-immunoprecipitation of NCAPH2-Halo with MCPH1-GFP. Nuclear extracts were prepared from *Ncaph2*$^{Halo/Halo}$, *Ncaph2*$^{Halo/Halo}$*Mcph1*$^{GFP/GFP}$ and *Ncaph2*$^{Halo/Halo}$*Mcph1*$^{\Delta cenGFP/\Delta cenGFP}$ cells. Immunoprecipitation was performed using GFP-trap agarose beads and analysed by in-gel detection of NCAPH2-Halo using the Halo-ligand TMR or by western blot using an anti-NCAPD3 antibody (IP-GFP). 5% of the lysate used for IP was loaded as input control. Anti-Lamin B1 antibody was used as a loading control. **(D,E)** Immunofluorescence analysis of the chromatin organisation

in *Ncaph2*$^{Halo/Halo}$*Mcph1*$^{GFP/GFP}$ and *Ncaph2*$^{Halo/Halo}$*Mcph1*$^{\Delta cenGFP/\Delta cenGFP}$ cells. MCPH1-GFP is only detected in the cell nucleus enriched in dots colocalising with some γH2AX foci (D). The deletion of its central domain induces a similar condensation of interphasic chromosomes as the one observed after the complete loss of function of *Mcph1* (E).

Figure 7. *MCPH1 has little effect on condensin II ATP hydrolysis and DNA binding*. **(A)** ATPase rate of condensin II complex in the presence of MCPH1. Q refers to condensin II with an ATPase deficient mutation in the Q-loop. Below is an SDS page gel of the completed reaction. Error bars indicate standard deviation from three repeats. **(B)** EMSA assay of MBP, MCPH1$_{1-435}$-MBP and -MCPH1$_{195-435}$-MBP using 50 bp of Cy5 labelled dsDNA. **(C)** EMSA assay of condensin II in the presence of MBP or MCPH1$_{1-435}$-MBP. **(D)** EMSA assay of condensin II in the presence or absence of 5FAM-MCPH1 peptide. Top image detecting Cy5 and bottom imaged detecting 5FAM.

Figure 8. *MCPH1 prevents the association of condensin II with chromosomes*. **(A)** Cartoon summarizing the experimental procedure corresponding to panel B. **(B)** Wild-type mouse oocytes were injected at the GV stage with *in vitro* transcribed mRNA coding for H2B-mCherry alone to mark the chromosomes in magenta (Control) or in combination with MCPH1 (+MCPH1). Meiosis I progression was followed by live cell confocal imaging. The segregation defects observed in the presence of MCPH1 are indicated by a yellow arrowhead. Maximum intensity z projection images of the main time points are shown between 3.3 h post GVBD onwards (number of oocytes analysed in three independent experiments: control :12; +MCPH1: 19). **(C)** Cartoon summarizing the experimental procedure corresponding to panel D. **(D)** Oocytes from

795 *Ncaph2$^{f/f}$ Tg(ZP3Cre)* females were injected at the GV stage with mRNA coding for
796 H2B-mCherry, MAD2 and NCAPH2-GFP only (control) or in combination with MCPH1
797 (+MCPH1) or MCPH1 deleted of the first N-terminal 200 amino acids (+MCPH1 Δ200).
798 Oocytes were arrested 16 h after GVBD in metaphase I owing to MAD2
799 overexpression, and maximum-intensity z projection images of chromosomes were
800 acquired by live cell confocal imaging (Total number of oocytes analysed in three
801 experiments: control: 37, +MCPH1: 58, +MCPH1Δ200: 12). **(E)** Quantification of
802 NCAPH2-GFP signal on the chromosomes. (Number of oocytes analysed in two
803 independent experiments: control: 11; +MCPH1: 14). Scale bar, 5 μm
804
805 **Figure 9**. *The closure of the SMC2-NCAPH2 interface prevents MCPH1 inhibitory*
806 *effect.* **(A)** Schematic representation of the protein fusion between SMC2 C-terminus
807 and the N-terminus of NCAPH2 using a linker comprising three TEV protease
808 cleavage sites. **(B)** Cartoon summarizing the experimental procedure corresponding
809 to panel C. **(C)** Oocytes from *Ncaph2$^{f/f}$ Tg(ZP3Cre)* females were injected at the GV
810 stage with mRNA coding for H2B-mCherry and MCPH1 in combination with NCAPH2-
811 GFP (NCAPH2-GFP+MCPH1) or with the fusion (Fusion-GFP+MCPH1). Meiosis I
812 progression was followed by live cell confocal imaging. Maximum intensity z-
813 projections images of the time points corresponding to anaphase I when segregation
814 defects are observed (total number of oocytes analysed in three experiments:
815 NCAPH2-GFP+MCPH1: 17, Fusion-GFP+MCPH1: 18). **(D)** Cartoon summarizing the
816 experimental procedure corresponding to panel E. **(E)** Oocytes from *Ncaph2$^{f/f}$*
817 *Tg(ZP3Cre)* females were injected at the GV stage with mRNA coding for H2B-
818 mCherry, MAD2 and Fusion-GFP only or in combination with TEV protease. Oocytes
819 were arrested 16 h after GVBD in metaphase I owing to MAD2 over-expression and

820 maximum-intensity z-projection images of chromosomes were acquired by live cell
821 confocal imaging. **(F)** Quantification of Fusion-GFP signal on the chromosomes (Total
822 number of oocytes analysed in three experiments: Fusion: 9; Fusion + MCPH1: 14,
823 Fusion + TEV: 13, Fusion + TEV + MCPH1: 18). Scale bar, 5 μm.
824
825 **Figure 10**. *Mcph1 deletion induces the coiling of the vermicelli*. **(A)**
826 Immunofluorescence analysis of the chromatin organisation in the four conditions:
827 wild-type, Δ*Wapl*, Δ*Mcph1* and Δ*Wapl* Δ*Mcph1*. In order to compare cells that are in
828 G2, prophase or metaphase, Histone H3-serine 10 (cyan) was used as a cell cycle
829 marker. The localization of SCC1-Halo was analysed using Halo-JFX554, NCAPH2-
830 GFP using nanobodies and DNA was detected using DAPI. **(B)** Magnified view of cells
831 marked with a white star in panel A. Scale bar, 5 μm.
832
833 **Figure 11.** *Super-resolution 3D-SIM analysis of G2 and metaphase cells deleted for*
834 *Wapl or both Mcph1 and Wapl*. **(A)** Cells deleted for Δ*Wapl* or Δ*Wapl*+Δ*Mcph1* in G2
835 or metaphase (M) were analysed by 3D-SIM. Maximum intensity projections of 16
836 consecutive mid sections covering 2 μm in depth. The left panel shows DNA coloured in
837 magenta and SCC1-Halo in green. The right panel shows the SCC1 signal with z-depth
838 colour-coded. Scale bar, 5 μm (inset, 1 μm) **(B)** Representative SCC1-Halo solenoid
839 structure corresponding to one chromosome from a Δ*Wapl*+Δ*Mcph1* cell in G2 was
840 segmented (green) and overlaid to the DNA (magenta). Scale bar, 2 μm. **(C)** 3D
841 surface rendering of the segmented and isolated solenoid from panel B. View from the
842 top, right, left and bottom of one segmented solenoid. Scale bar, 1 μm.
843
844

SUPPLEMENTARY FIGURE LEGENDS

Supplementary figure 1. *The cell cycle parameters are unchanged in Mcph1 deleted cells.* FACS analysis of the cell cycle parameters of *Mcph1* deleted cells compared to wild type: **(A)** Analysis of the DNA content using propidium Iodide (repeated twice). **(B)** EdU incorporation (repeated twice). **(C)** H3 Phosphorylation on serine 10 (repeated twice). **(D)** Western blot analysis of the amount of γH2AX and H3 phosphorylation on serine 10 in wild-type cells compared to *Mcph1* deleted cells. Scale bar, 5 μm.

Supplementary figure 2. *Chromocenters disruption in Mcph1 deleted cells*. Immunofluorescence analysis of centromere clustering using CREST antibody showing that in *Mcph1* deleted cells, the centromeres are scattered in the nucleus even in replicating, EdU-positive cells.

Supplementary figure 3. *Mcph1 deletion decreases intra-compartment strength and does not affect looping.* **(A)** Pearson correlation map at 250 kB for wildtype and *Mcph1* deletion maps for the intrachromosomal region of chromosome 11 (wildtype below diagonal). **(B)** Pearson correlation map at 250 kB for wildtype and *Mcph1* deletion maps for the intrachromosomal region of chromosome 11 sorted by values of the principal eigenvector (wildtype below diagonal). Intra-compartmental interactions (A-A and B-B) vs inter-compartment interactions (A-B) show a relative decrease in the *Mcph1* deletion maps. **(C)** Aggregate peak analysis using the loop lists for both wildtype and mcph1 deletion on both Hi-C maps shows no significant global change to chromatin looping, which is also verified by direct observation of the maps.

Supplementary figure 4. *Condensin I does not interact with MCPH1.* **(A)** Strep-tag pull-down assay indicating strep tagged condensin I does not pull-down any MBP-MCPH1 construct. SDS page visualised with Coomassie stain for input samples and silver stain for resin samples. **(B)** Condensin II and MBP-MCPH1$_{196-435}$ form a stable complex and co-elute in size exclusion chromatography. Elution profiles of condensin II + MBP-MCPH1$_{196-435}$, condensin II alone and MBP-MCPH1$_{196-435}$ alone are shown in green, blue and red respectively. Fractions from void, condensin II and MCPH1 peak were run on an SDS page and stained with Coomassie. **(C)** Sequence conservation map of MCPH1$_{1-435}$ generated using the ConSurf server [46,47], with the central motif indicated. Colours range from non-conserved (green) to conserved (purple), 'b' indicates residues predicted to be buried and 'e' indicates residues predicted to be solvent-exposed.

Supplementary figure 5. *Western blot analysis of the four conditions analysed in Figures 10 and 11*. The first cell line is: *Ncaph2*$^{GFP/GFP}$ *Scc1*$^{Halo/Halo}$ *Wapl*$^{TevLox/\Delta}$ *Mcph1*$^{wt/wt}$. The second cell line is: *Ncaph2*$^{GFP/GFP}$ *Scc1*$^{Halo/Halo}$ *Wapl*$^{TevLox/\Delta}$ *Mcph1*$^{\Delta/\Delta}$. *Wapl* can be deleted in both cell lines after Tamoxifen treatment giving four experimental conditions: Wild type, Δ*Wapl*, Δ*Mcph1* and Δ*Wapl* Δ*Mcph1*.

MATERIAL AND METHODS

Mouse strain, *in vitro* culture and oocytes micro-injection.

Ncaph2$^{tm1a(EUCOMM)Wtsi}$ (MBCH;EPD0070-2-G090) were obtained from the Wellcome Trust Sanger Institute. The corresponding *flox* allele was obtained as previously described [52]. The fusion was obtained by cloning in frame *Smc2* cDNA, a linker containing three TEV protease cleavage sites (GGGGSGGGSGGGGTGSENLYFQGPRENLYFQGGSENLYFQGTRGGGGSGGG GSGGGG), *Ncaph2* cDNA (Origene, MC200537) and the eGFP ORF in the pUC19 vector.

Fully grown prophase-arrested GV oocytes were isolated and injected with mRNAs (5–10 pl) diluted in RNase-free water at the following concentrations: H2B–mCherry: 150 ng μl^{-1}, Mad2: 200 ng μl^{-1}, NCAPH2–eGFP: 50 ng μl^{-1}, Fusion-EGFP (50 ng μl^{-1}), MCPH1 (200 ng μl^{-1}), TEV protease: 250 ng μl^{-1}. All experimental procedures were approved by the University of Oxford ethical review committee and licensed by the Home Office under the Animal (Scientific procedures) Act 1986. No statistical method was used to predetermine sample size. The experiments were not randomised and the investigators were not blinded to allocation during experiments and outcome assessment.

Live cell confocal imaging.

Oocyte live cell imaging was done in 4-well Labtek chambers (ref. 155383) in 4 µl drops of M16 medium covered with mineral oil (Sigma) in a 5% CO_2 environmental microscope incubator at 37 °C (Pecon). Images were acquired using an LSM-780 confocal microscope (Zeiss) using the ZEN 2011 software. Between 7 and 12 slices (between 1 and 4 µm) were acquired every 5 to 15 min for each stage position using

914 the autofocus tracking macro developed in J. Ellenberg's laboratory at EMBL. For
915 detection of eGFP and mCherry, 488-nm and 561-nm excitation wavelengths and
916 MBS 488/561 filters were used. Images were further analysed using Volocity software.
917 For high-resolution videos, the lens used was a C-Apochromat ×63/1.20 W Corr UV–
918 VIS–IR. The fluorescence was quantified using Fiji.

919 **E14 mouse embryonic stem cells culture**

920 E14 mouse embryonic stem cells were grown in Dulbecco's modified Eagle's medium
921 (DMEM; Life Technologies) supplemented with 10% foetal calf serum (Seralab),
922 2 mM L-glutamine (Life Technologies), 1x non-essential amino acids (Life
923 Technologies), 50 µM β-mercaptoethanol (Life Technologies), 1X penicillin-
924 streptomycin solution (Life Technologies) and leukaemia inhibitory factor (LIF) made
925 in-house. All E14 cells were grown in feeder-free conditions on gelatinised plates at
926 37 °C in a humid atmosphere with 5% CO_2.
927 For conditional deletion of *Wapl*, Cre recombinase was induced by treating the cells
928 with 800 nM 4-hydroxytamoxifen (OHT) for the indicated time. The degradation of
929 NCAPH2-HALO was triggered by adding HaloTag® PROTAC Ligand (Promega) at
930 1µM for 16 hours.
931 The Halo Ligands (Halo-TMR Ligand, Promega, Ref G8251) were added in the culture
932 medium for 20 min at 100 nM. Cells were washed and left in the incubator with fresh
933 medium for an extra 30 min to remove the unbound ligand before being analysed by
934 immunofluorescence or western blot.
935

936 **Genomic engineering using CRISPR Homology-directed repair**

The sgRNAs were designed using the CRISPOR online tool (http://crispor.tefor.net/crispor.py) and cloned in the pSptCas9(BB)-2A-Puro(PX459)-V2.0 vector (Addgene #62988). The sgRNA cloning was done according to the protocol from [66].

To generate the targeting constructs, 1 kb homology arms were amplified by PCR (Q5-NEB) from E14 cells genomic DNA and cloned in pUC19 vector using Gibson Assembly Master Mix kit (New England Biolabs). The targeting construct was designed such that the guide RNA sequence used for the specific targeting was interrupted by the tag or contained silent mutations.

For each targeting, a 6 cm dish of E14 cells 50% confluent was transfected using 2μg of pX459-Cas9-sgRNA and 5 μg of targeting construct using Lipofectamine 2000 (ThermoFisher) according to manufacturer's guidelines. The next day, cells were trypsinised and plated at three different densities in 20 cm dishes in medium supplemented with puromycin (1 μg/ml). The selection medium was removed 48 h later and cells were grown for approximately ten days. 96 Individual clones were then picked in 96 well plates, grown for 48 h and split into two 96 well plates. The next day, genomic DNA was prepared using 50 μl of Lysis buffer (10 mM Tris HCl pH8, 1 mM EDTA, 25 mM NaCl, 200 μg/ml Proteinase K), incubated at 65 °C for 1 h, 95 °C for 10 min to inactivate Proteinase K. The clones were then screened by PCR (Q5-NEB) and amplified to be further analysed by western blot.

Conditional Wapl deletion

To generate the TEV protease conditional cells, a series of four tandem STOP cassette (Addgene, pBS.DAT-LoxStop, Jacks Lab) flanked by two LoxP sites was cloned between the pCAG promoter and the PK tagged TEV protease cDNA. The

962 CRE-ERT2 cDNA was cloned upstream under the transcriptional control of the
963 Rosa26 Splice acceptor. This construct was then flanked by 1 kb homology arms to
964 target the construct at the Rosa26 locus using CRISPR-HDR. After selecting and
965 amplifying of the targeted E14 clones, the TEV protease could be detected by western
966 blot 8 h post hydroxytamoxifen induction. Immunofluorescence analysis revealed a
967 homogeneous expression of TEV protease in all the cells.
968 In the selected clones, three TEV protease cleavage sites were targeted in Wapl
969 coding sequence after Proline 499 using CRISPR-HDR. After selecting of the targeted
970 clones, it appeared that TEV cleavage of the Wapl protein led to a new steady-state
971 in the cells in which a small amount of full-length protein was present preventing the
972 formation of vermicelli. To avoid this compensation effect, we targeted loxP sites in
973 the *Wapl* gene on both sides of exon 4 to induce the deletion of the gene
974 simultaneously as the TEV cleavage of the protein already present in the cell. This
975 combined strategy induced a complete loss of function of *Wapl* within 8 hours and the
976 formation of vermicelli.
977
978 **sgRNA used for CRISPR-HDR**

Targeted Gene	sgRNA
NCAPH2-GFP	GGTGGAAAGTAGTATATACC
NCAPH2-Halo	GGTGGAAAGTAGTATATACC
MCPH1 deletion Sg5'	GGTGTGCAATTCCTAGTGTG
MCPH1 deletion Sg3'	AGCTGTTCCTTAGAACACGA
MCPH1-GFP	ACAGTGAGACATCTACAATG
STOP-TEV	CATGGATTTCTCCGGTGAAT
WAPL-Lox-TEV Sg5'	AATGGGTGCTTATAATTAGC

WAPL-Lox-TEV Sg3'	ACAATGTCACAATGGCTCAT
SCC1-Halo	ATAATATGGAACCGTGGTCC
DELCEN-MCPH1	CGTTGAGGCTTCTTCCTATG
TEV sites in Wapl Two Guide RNA used in combination	 AATGGGTGCTTATAATTAGC ACAATGTCACAATGGCTCAT

Immunofluorescence detection

E14 cells were plated on glass coverslips (Marienfeld, High precision, 22x22, N°1.5H, Ref 0107052) in 6-well plates. 48 h later, cells were labelled with the Halo Ligand (Halo-JFX554, Janelia 100 nM 30 min) [67] or EdU (5 min at 10 μM), washed PBS and then fixed in 3.8% Formaldehyde (Sigma-F8775) in PBS for 15 min. After three PBS washes, cells were permeabilised in 0.5% Triton X-100 in PBS for 10 min and then washed three times in PBS. After 20 min in blocking buffer: PBS 3% BSA (Sigma, A4503). The coverslips were transferred in a wet chamber and covered with 100 μl of antibody solution in blocking buffer. After 1 h at room temperature, the coverslips were washed three times in blocking solution and incubated with the secondary antibody for 1 h (AlexaFluor 594 or 488, 1/500, Life Technology). After three washes in PBS, DNA was labelled using Hoechst (Sigma, 33342, 5 μg/ml) for 15 min. The coverslips were then washed in PBS, mounted in Vectashield (H1000) and sealed using nail varnish. Imaging was done using an LSM 780 confocal microscope (Zeiss) using the ZEN 2011 software. EdU was detected according to the manufacturer's instruction (Click-iT EdU Imaging kit, Invitrogen). CDK1 inhibition was performed by incubating the cells in E14 medium supplemented with 9 μM RO-3306 (SIGMA SML0569) for 7 h before fixation.

Immunoprecipitation and western blot

The cells were collected using Trypsin and washed in PBS twice. The cell pellet was resuspended in 10 vol. of buffer A (10 mM HEPES pH7.9, 1.5 mM MgCl2, 10 mM KCl, 1 mM DTT, 1 mM PMSF, 1x complete protease inhibitor (Roche, 04693132001) and incubated 15 min on ice. After centrifugation at 4°C at 2000 rpm for 5 min to remove the supernatant, the pellet was resuspended in 3 vol. of buffer A + NP40 (0.1%) and incubated for 15 min on ice followed by another centrifugation at 4 °C 4000 rpm for 5min to remove the supernatant and resuspended in lysis buffer: (20 mM Tris pH7.5, 200 mM NaCl, 1% Triton X-100, 0.1% sodium deoxycholate, 1 mM DTT, 1 mM PMSF, 1x complete protease inhibitor (Roche, 04693132001), 1x super nuclease). The suspension was passed through a 26GA needle 10 times, left on ice for 1 h and centrifuged at 20000g for 30min. Proteins were quantified by Bradford (KitBiorad 5000006, spectrophotometer BIOCHROM). Each IP was performed using 1 mg of protein in 1 ml in lysis buffer. GFP-Trap agarose beads (GTA-10, Chromotek) were washed in lysis buffer and incubated according to the supplier's instructions with the protein extract overnight at 4 °C. Washed five times in Lysis buffer and separated by SDS-PAGE, imaged using Fujifilm FLA-7000 imager if Halo ligand was used and then transferred overnight on Nitrocellulose membrane. After Ponceau red evaluation of the transfer quality, the membrane was blocked in PBS-0,1%Tween 20 + 5% non-fatty milk for an hour and incubated with the antibody overnight in PBS-0,1%Tween 20 + 5% non-fatty milk. Western blots were analysed using LI-COR Odyssey Fc imager.

Antibodies list

NCAPH2: Rabbit polyclonal produced on demand by Eurogentec (WB:1/1000).

SCC1: Millipore, 53A303, mouse monoclonal antibody (WB:1/1000).

SMC2: Cell Signaling Technology, D23C5, rabbit monoclonal Antibody (WB:1/500).

Lamin B1: Abcam Ab133741, rabbit monoclonal (WB:1/1000).

MCPH1: Cell Signaling Technology, D38G5, rabbit monoclonal Antibody (WB:1/1000).

CREST: Immunovision HCT0-100, human autoantibody (IF: 1/500)

H3PS10: Millipore, clone 3H10, mouse monoclonal (WB:, IF:1/2000).

γH2aX: Millipore, clone JBW301, mouse monoclonal (WB:, IF:1/500).

CDK1: Cell Signaling Technology, cdc2, 77055, rabbit polyclonal (WB:1/1000).

Phospho-CDK1: Cell Signaling Technology, phospho-cdc2 (Tyr15) antibody, 9111, rabbit polyclonal (WB:1/1000).

WAPL: provided by J.M. Peters's Lab (WB:1/1000).

GFP: Abcam, ab290, rabbit polyclonal (WB: 1/1000, IF:1/500).

PK-Tag: Biorad, MCA 1360G, mouse monoclonal (WB:1/1000).

Cyclin B1: Cell Signaling Technology, 4138T, rabbit monoclonal (IF:1/200).

NCAPD3: Bethyl Laboratory, A300-604A-M, rabbit polyclonal (WB:1/1000).

Halo in gel imaging

Cells were incubated with Halo-TMR ligand (100 nM) for 30 min then washed in ligand-free medium and analysed by immunofluorescence or for protein purification. After SDS-PAGE, the fluorescence was measured in the gel using an Imager Fujifilm FLA-7000.

FRAP

Live-cell imaging was performed in a spinning disk confocal system (PerkinElmer UltraVIEW) with an EMCCD (Hamamatsu) mounted on an Olympus IX8 microscope with Olympus 60x 1.4 N.A. and 100x 1.35 N.A. objectives. Image acquisition and

quantitation were performed using Volocity software. During imaging, cells were maintained at 37°C and 5% CO2 in a humidified chamber. FRAP was carried out with a 488 nm laser beam, 100% power, 15–30 ms. The fluorescence intensity measurement was performed by using ImageJ. All signals were subjected to background correction. The fluorescence intensity of unbleached and bleached areas was normalized to that of initial pre-bleaching images using the EasyFRAP website.

In-situ Hi-C

Hi-C libraries were generated as described in [68], analysed using the Juicer pipeline [69] and visualised with Juicebox [70]. We sequenced 785,454,085 Hi-C read pairs in wild-type mouse ES cells, yielding 509,278,039 Hi-C contacts; we also sequenced 1,814,815,287 Hi-C read pairs in *Mcph1* deleted cells, yielding 1,284,169,272 Hi-C contacts. Loci were assigned to A and B compartments at 100 kB resolution. Loops were called with HiCCUPS at 25 kB, 10 kB, and 5 kB resolution. Contact domains were called at 10 kB resolution. Contact frequency analysis was performed as described in [71]. All code used for these analyses is publicly available at (github.com/aidenlab), with a help forum for questions at (aidenlab.org/forum.html).

Structured illumination microscopy

Super-resolution 3D-SIM was performed on a DeltaVision OMX SR system (GE Healthcare) equipped with sCMOS cameras (PCO) and 405, 488 and 568 nm lasers, using a 60x NA 1.42 PlanApo oil immersion objective (Olympus). To minimise artefacts due to spherical aberration

Raw data sets were acquired with a z-distance of 125 nm and 15 raw images per plane (5 phases, 3 angles). Reconstructions were performed with SoftWoRx 6.2 (GE Healthcare) using channel-specifically measured optical transfer functions (OTFs)

generated from 100 nm diameter green and red FluoSphere beads (ThermoFisher), respectively, and Wiener filter set to 0.0030. For DAPI acquisitions, the sample was excited with the 405 nm laser and the emission detected in the green channel and reconstructed with a green OTF. This is enabled by the broad emission spectrum of DAPI and empirically resulted in better reconstructions than reconstructing blue emission with a 'blue' OTF obtained typically less intense blue FluoSphere beads.

All data underwent quality assessment via SIMcheck [72] to determine image quality via analysis of modulation contrast to noise ratio (MCNR), spherical aberration mismatch, reconstructed Fourier plot and reconstructed intensity histogram values. Reconstructed 32-bit 3D-SIM datasets were thresholded to the stack modal intensity value and converted to 16-bit composite z-stacks to discard negative intensity values using SIMcheck's "threshold and 16-bit conversion" utility and MCNR maps were generated using the "raw data modulation contrast" tool of SIMcheck. To eliminate false positive signals from reconstructed noise, we applied SIMcheck's 'modulation contrast filter' utility. Briefly, this filter sets masks out all pixels, where the underlying MCNR value in the raw data fall below an empirically chosen threshold MCNR value of 6.0, followed by a Gaussian filter with 0.8 pixel radius (xy) to smoothen hard edges [73].

Colour channels were registered in 3D with the open-source software Chromagnon 0.85 [74] determining alignment parameter (x,y,z-translation, x,y,z-magnification, and z-rotation) from a 3D-SIM dataset acquired on the date of image acquisition of multicolour-detected 5-ethenyl-2'-deoxyuridine (EdU) pulse replication labelled C127 mouse cells serving as biological 3D alignment calibration sample [75].

FACS

Cells were incubated with EdU (10 μM) for 5 min, collected using trypsin, washed with PBS and fixed in 3.8% Formaldehyde (Sigma-F8775) in PBS for 15 min. After three PBS washes, cells were permeabilised in 0.5% Triton X-100 in PBS for 10 min and then washed three times in PBS. Cells were then incubated for 20 min in blocking buffer: PBS 3% BSA (Sigma, A4503), incubated for 1 h with H3PS10 antibody (1/1000), washed three times in PBS and then incubated with fluorescent secondary antibody (Alexa Fluor 488, 1/500, Life Technology) incubated with propidium iodide (Sigma, 30 μg/ml) and then analysed by FACS. 15,000 cells were analysed for each data point. EdU detection was done following the manufacturer's instruction (Click-iT EdU Imaging kit, Invitrogen).

Protein purification

Human condensin II pentameric and tetrameric complexes were purified as previously described [59]. Full length MCPH1 was cloned into the pLIB vector and viral bacmids were generated using Tn7 transposition in DH10EMBacY cells (Geneva biotech), transfected into Sf9 cells using Cellfectin II (GIBCO) and resultant virus harvested after 3 days. Virus was further amplified in Sf9 cells before being used to infect High Five cells for protein expression. High Five cells were harvested by centrifugation 3 days after infection. Cell pellets were resuspended in purification buffer (20 mM HEPES pH 8, 300 mM KCl, 5 mM $MgCl_2$, 1 mM DTT, 10% glycerol) supplemented with 1 Pierce protease inhibitor EDTA-free tablet (Thermo Scientific) per 50 mL and 25 U/ml of Benzonase (Sigma) and lysed with a Dounce homogenizer followed by brief sonication. The lysate was cleared with centrifugation, loaded onto a StrepTrap HP (GE), washed with purification buffer and eluted with purification buffer supplemented with 5 mM desthiobiotin (Sigma). Size exclusion chromatography was performed

using purification buffer on a Superdex 200 16/60 column (GE), and protein containing fractions separated from the void volume were pooled and concentrated.

MCPH1 residue 1-435, 1-195 and 196-435 were cloned into a pET vector with an N-terminal 6xHis-MBP fusion tag or with an N-terminal 6xHis and C-terminal MBP tag, and expressed in *E. coli* BL21 (DE3) pLysS cells (Novagen). Cells were grown at 37 °C, induced with 1 mM IPTG for 4 h, before being harvested by centrifugation and flash frozen. The cell pellet was resuspended in MCPH1 purification buffer (20 mM Tris pH 7.5, 150 mM NaCl, 10% glycerol, 1 mM DTT, Pierce protease inhibitor EDTA-free tablet), lysed with sonication on ice, treated with Benzonase (Sigma-Aldrich) (10 µL per 100 mL, with 1 mM $MgCl_2$) and cleared via centrifugation. Cleared cell lysate was filtered with a 5 µm filter, imidazole was added to a final concentration of 10 mM and incubated with pre-equilibrated His-Pure NTA resin. The resin was washed with MCPH1 purification buffer, then washed with wash buffer 20 mM Tris pH 7.5, 500 mM NaCl, 20 mM imidazole, before elution with 20 mM Tris pH 8, 300mM NaCl, 500 mM Immidazole, 10% glycerol. Protein was diluted 2-fold with buffer TA (20 mM Tris pH 8, 5% glycerol, 1 mM DTT), and loaded onto a HiTrap Q Fast Flow column or loaded on to HiTrap Heparin HP column (GE) and eluted with a gradient of buffer TB (20 mM Tris pH 8, 2 M NaCl, 5% glycerol, 1 mM DTT). For protein used in ATPase assays, final size exclusion chromatography was performed using purification buffer and a Superdex 200 10/300 or 16/60 column (GE).

Pull-downs

Condensin complexes (0.1 µM) were mixed with at least a 10-fold molecular excess of MBP MCPH1 constructs or MBP protein in 200 µL and incubated with 40 µL of Strep-tactin sepharose resin (IBA) in MCPH1 purification buffer. The resin was

washed 5 times, before being eluted by boiling in 1x NuPAGE LDS sample buffer with 50 mM DTT. Samples of 10% input and resin elution were run on 4-12% NuPAGE Bis-Tris gels against Color Prestained Protein Standard, Broad Range (NEB) and stained with Instant Blue (Expedeon) or silver stain (Life Technology).

The absence of the CAP-D3 subunit was confirmed by western blot analysis of the output protein samples. For this, the tetrameric condensin II pull-down was run on an SDS page gel and transferred to a nitrocellulose membrane (Amersham). The membrane was then blocked with 5% milk-powder in TBS-T, before being probed with a mouse anti-CAP-D3 antibody (Santa Cruz, Sc-81597, used at 1/1000), then a goat DyLight 800 florescent anti-mouse secondary antibodies (Cell Signaling Technology, 5257, used at 1/5000). The membrane was imaged using a LI-COR imager.

Fluorescence polarisation assays

Peptides used in fluorescence polarization assays were synthesised by Genscript and are shown in Table 1. The concentration of 5FAM wild-type MCPH1$_{407-422}$ was determined using the 5-FAM extinction coefficient of 83,000 $(cmM)^{-1}$ at 493 nm. Non-labelled peptides had TFA removed to less than 1% and were accurately quantified using Genscript's amino acid analysis service. All peptides were solubilised in DMSO and diluted to a working concentration in FP assay buffer (20 mM Tris pH 7.5, 200 mM NaCl, 1 mM DTT). Peptides in competition experiments were diluted in a two-fold series with FP assay buffer supplemented with DMSO, such that DMSO concentration was constant for all peptide concentrations.

Table 1: Peptides used in FP experiments

Name	Sequence

5FAM-MCPH1$_{407-422}$	5FAM- CGESSYDDYFSPDNLKER
MCPH1$_{407-422}$	CGESSYDDYFSPDNLKER
MCPH1$_{407-422}$pS417	CGESSYDDYF{pSER}PDNLKER

FP binding assays were performed with 0.3 μM of 5-FAM labelled wild-type MCPH1$_{407-422}$ and 0.625, 1.25, 1.75, 2.5, 3.5 and 5 μM of pentameric condensin II or tetrameric condensin II lacking the CAPG2 subunit, in a total volume of 40 μl in half-area black plates (Constar). The plate was incubated at room temperature for 20 min, before being read with an Omega plate reader (BMG Labtech) at 5 min intervals and monitored to ensure binding had reached equilibrium. Each plate was read three times, and three replicates were performed at each protein concentration.

FP competition titrations were performed as above, but with 0.63 μM of condensin II, 0.3 μM of 5FAM-MCPH1$_{407-422}$ and indicated amount of competing peptide. Data was normalised by subtracting the FP signal for 5FAM-MCPH1$_{407-422}$ in the absence of condensin II at each peptide concentration and divided by the background-subtracted signal of sample with 0.63 μM of condensin II and 0.3 μM of 5FAM-MCPH1$_{407-422}$ without any competing peptide. Each plate was read 4 times and each experiment was performed a total of 3 times.

Fluorescence polarisation data was fit using equations for direct binding and directly competitive binding, as presented by [76].

ATPase assays

Complexes of wild type or ATPase hydrolysis deficient Q-loop mutants condensin II with MCPH1$_{1-435}$MBP were purified with gel filtration on a Superose 6 10/300 column, along with wild-type only control in ATPase assay buffer (20 mM Tris pH 7.5, 150 mM

NaCl, 1 mM DTT). Prior to gel-filtration all samples were treated with Tev protease to remove N-terminal 6x His-tag on MCPH1$_{1-435}$MBP. ATPase assays were performed using the EnzChek™ Phosphate Assay Kit (Invitrogen) modified for a 96 well plate format [77]. 50 bp double stranded DNA sequence with the same as that used in the EMSA (without a fluorescent label). Reactions contained 50 nM protein with or without 800 nM DNA. Final conditions included 1 mM ATP and a total salt concentration of 50 mM. Protein/DNA was preincubated in reaction mix without ATP for 15 minutes at room temperature before the reaction was started by addition of ATP immediately before putting it in the plate reader to track phosphate release. A standard curve ATPase rate was determined from a linear fit of data from the first 60 min.

Electromobility shift assays

EMSAs were performed using 50 nM of 50 bp double stranded DNA labelled with Cy5 at the 5' with the sequence:

CTGTCACACCCTGTCACACCCTGTCACACCCTGTCACACCCTGTCACACC

For MCPH1 EMSAs, MCPH1-MBP constructs were diluted in 20 mM Tris pH 7.5, 150 mM NaCl, 10% glycerol, 1 mM DTT and mixed 1 in 2 with DNA in 20 mM HEPES pH 8, 300 mM KCl, 5 mM $MgCl_2$, 10% glycerol and 1 mM DTT.

For condensin II/MCPH1 EMSAs, condensin II diluted in 20 mM HEPES pH 8, 300 mM KCl, 5 mM $MgCl_2$, 10% glycerol and 1 mM DTT and mixed with MCPH1$_{1-435}$-MBP, MBP or 5-FAM-MCPH1$_{407-424}$ diluted in in 20 mM Tris pH 7.5, 150mM NaCl, 10% glycerol, 1 mM DTT. DNA was then added to a final concentration of 50 nM. Protein and DNA were incubated on ice for 15 min, before being loaded in a 2% agarose gel and run in 0.5x TBE buffer for 30 min. Gel was imaged using a Typhoon.

REFERENCES

1. Yatskevich, S., Rhodes, J. & Nasmyth, K. Organization of Chromosomal DNA by SMC Complexes. *Annu. Rev. Genet.* **53**, 445–482 (2019).
2. Tedeschi, A. *et al.* Wapl is an essential regulator of chromatin structure and chromosome segregation. *Nature* **501**, 564–568 (2013).
3. Challa, K. *et al.* Meiosis-specific prophase-like pathway controls cleavage-independent release of cohesin by Wapl phosphorylation. *bioRxiv* 1–27 (2018) doi:10.1101/250589.
4. Hill, L. *et al.* Wapl repression by Pax5 promotes V gene recombination by Igh loop extrusion. *Nature* **584**, 142–147 (2020).
5. Davidson, I. F. *et al.* DNA loop extrusion by human cohesin. *Science (80-.).* **366**, 1338–1345 (2019).
6. Ganji, M. *et al.* Real-time imaging of DNA loop extrusion by condensin. *Science (80-.).* **360**, 102–105 (2018).
7. Wutz, G. *et al.* ESCO1 and CTCF enable formation of long chromatin loops by protecting cohesinstag1 from WAPL. *Elife* **9**, 1–33 (2020).
8. Gerlich, D., Hirota, T., Koch, B., Peters, J. M. & Ellenberg, J. Condensin I stabilizes chromosomes mechanically through a dynamic interaction in live cells. *Curr. Biol.* **16**, 333–344 (2006).
9. Hansen, A. S., Pustova, I., Cattoglio, C., Tjian, R. & Darzacq, X. CTCF and cohesin regulate chromatin loop stability with distinct dynamics. *Elife* **6**, 1–33 (2017).
10. Cutts, E. E. & Vannini, A. Condensin complexes: understanding loop extrusion one conformational change at a time. *Biochem. Soc. Trans.* **48**, 2089–2100 (2020).

11. Hirota, T., Gerlich, D., Koch, B., Ellenberg, J. & Peters, J. M. Distinct functions of condensin I and II in mitotic chromosome assembly. *J. Cell Sci.* **117**, 6435–6445 (2004).

12. Ono, T. *et al.* Differential contributions of condensin I and condensin II to mitotic chromosome architecture in vertebrate cells. *Cell* **115**, 109–121 (2003).

13. Ono, T., Fang, Y., Spector, D. L. & Hirano, T. Spatial and Temporal Regulation of Condensins I and II in Mitotic Chromosome Assembly in Human Cells. *Mol. Biol. Cell* **15**, 3296–3308 (2004).

14. Walther, N. *et al.* A quantitative map of human Condensins provides new insights into mitotic chromosome architecture. *J. Cell Biol.* **217**, 2309–2328 (2018).

15. Gibcus, J. H. *et al.* A pathway for mitotic chromosome formation. *Science (80-.).* **359**, (2018).

16. Baxter, J. & Aragón, L. A model for chromosome condensation based on the interplay between condensin and topoisomerase II. *Trends Genet.* **28**, 110–117 (2012).

17. Elbatsh, A. M. O. *et al.* Cohesin Releases DNA through Asymmetric ATPase-Driven Ring Opening. *Mol. Cell* **61**, 575–588 (2016).

18. Beckouët, F. *et al.* Releasing Activity Disengages Cohesin's Smc3/Scc1 Interface in a Process Blocked by Acetylation. *Mol. Cell* **61**, 563–574 (2016).

19. Chan, K. L. *et al.* Cohesin's DNA exit gate is distinct from its entrance gate and is regulated by acetylation. *Cell* **150**, 961–974 (2012).

20. Gligoris, T. G. *et al.* Closing the cohesin ring: Structure and function of its Smc3-kleisin interface. *Science (80-.).* **346**, 963–967 (2014).

21. Hassler, M. *et al.* Structural Basis of an Asymmetric Condensin ATPase Cycle.

Mol. Cell **74**, 1175-1188.e9 (2019).

22. Lee, B. G. *et al.* Cryo-EM structures of holo condensin reveal a subunit flip-flop mechanism. *Nat. Struct. Mol. Biol.* **27**, 743–751 (2020).

23. Buheitel, J. & Stemmann, O. Prophase pathway-dependent removal of cohesin from human chromosomes requires opening of the Smc3-Scc1 gate. *EMBO J.* **32**, 666–676 (2013).

24. Huis In't Veld, P. J. *et al.* Characterization of a DNA exit gate in the human cohesin ring. *Science (80-.).* **346**, 968–972 (2014).

25. Ono, T., Yamashita, D. & Hirano, T. Condensin II initiates sister chromatid resolution during S phase. *J. Cell Biol.* **200**, 429–441 (2013).

26. Schwarzer, W. *et al.* Two independent modes of chromatin organization revealed by cohesin removal. *Nature* **551**, 51–56 (2017).

27. Abe, S. *et al.* The initial phase of chromosome condensation requires Cdk1-mediated phosphorylation of the CAP-D3 subunit of condensin II. *Genes Dev.* **25**, 863–874 (2011).

28. Woods, C. G., Bond, J. & Enard, W. Autosomal recessive primary microcephaly (MCPH): A review of clinical, molecular, and evolutionary findings. *Am. J. Hum. Genet.* **76**, 717–728 (2005).

29. Thornton, G. K. & Woods, C. G. Primary microcephaly: do all roads lead to Rome? *Trends Genet.* **25**, 501–510 (2009).

30. Neitzel, H. *et al.* Premature chromosome condensation in humans associated with microcephaly and mental retardation: A novel autosomal recessive condition. *Am. J. Hum. Genet.* **70**, 1015–1022 (2002).

31. Trimborn, M. *et al.* Mutations in microcephalin cause aberrant regulation of chromosome condensation. *Am. J. Hum. Genet.* **75**, 261–266 (2004).

32. Trimborn, M., Schindler, D., Neitzel, H. & Hirano, T. Misregulated chromosome condensation in MCPH1 primary microcephaly is mediated by condensin II. *Cell Cycle* **5**, 322–326 (2006).

33. Yamashita, D. *et al.* MCPH1 regulates chromosome condensation and shaping as a composite modulator of condensin II. *J. Cell Biol.* **194**, 841–854 (2011).

34. Arroyo, M. *et al.* MCPH1 is essential for cellular adaptation to the G2-phase decatenation checkpoint. *FASEB J.* **33**, 8363–8374 (2019).

35. Arroyo, M. *et al.* MCPH1, mutated in primary microcephaly, is required for efficient chromosome alignment during mitosis. *Sci. Rep.* **7**, 1–12 (2017).

36. Venkatesh, T. & Suresh, P. S. Emerging roles of MCPH1: Expedition from primary microcephaly to cancer. *Eur. J. Cell Biol.* **93**, 98–105 (2014).

37. Leung, J. W. *et al.* SET nuclear oncogene associates with microcephalin/MCPH1 and regulates chromosome condensation. *J. Biol. Chem.* **286**, 21393–21400 (2011).

38. Cicconi, A. *et al.* Microcephalin 1/BRIT1-TRF2 interaction promotes telomere replication and repair, linking telomere dysfunction to primary microcephaly. *Nat. Commun.* **11**, (2020).

39. Lin, S. Y. & Elledge, S. J. Multiple tumor suppressor pathways negatively regulate telomerase. *Cell* **113**, 881–889 (2003).

40. Alderton, G. K. *et al.* Regulation of mitotic entry by microcephalin and its overlap with ATR signalling. *Nat. Cell Biol.* **8**, 725–733 (2006).

41. Gruber, R. *et al.* MCPH1 regulates the neuroprogenitor division mode by coupling the centrosomal cycle with mitotic entry through the Chk1-Cdc25 pathway. *Nat. Cell Biol.* **13**, 1325–1334 (2011).

42. Chang, H. Y. *et al.* Microcephaly family protein MCPH1 stabilizes RAD51

filaments. *Nucleic Acids Res.* **48**, 9135–9146 (2020).

43. Tibelius, A. *et al.* Microcephalin and pericentrin regulate mitotic entry via centrosome-associated Chk1. *J. Cell Biol.* **185**, 1149–1157 (2009).

44. Buster, D. W. *et al.* SCFSlimb ubiquitin ligase suppresses condensin II-mediated nuclear reorganization by degrading Cap-H2. *J. Cell Biol.* **201**, 49–63 (2013).

45. Nguyen, H. Q. *et al.* Drosophila Casein Kinase I Alpha Regulates Homolog Pairing and Genome Organization by Modulating Condensin II Subunit Cap-H2 Levels. *PLoS Genet.* **11**, 1–32 (2015).

46. Berezin, C. *et al.* ConSeq: The identification of functionally and structurally important residues in protein sequences. *Bioinformatics* **20**, 1322–1324 (2004).

47. Ashkenazy, H. *et al.* ConSurf 2016: an improved methodology to estimate and visualize evolutionary conservation in macromolecules. *Nucleic Acids Res.* **44**, W344–W350 (2016).

48. Van Roey, K. *et al.* Short linear motifs: Ubiquitous and functionally diverse protein interaction modules directing cell regulation. *Chem. Rev.* **114**, 6733–6778 (2014).

49. Oppermann, F. S. *et al.* Combination of chemical genetics and phosphoproteomics for kinase signaling analysis enables confident identification of cellular downstream targets. *Mol. Cell. Proteomics* **11**, 1–12 (2012).

50. Errico, A., Deshmukh, K., Tanaka, Y., Pozniakovsky, A. & Hunt, T. Identification of substrates for cyclin dependent kinases. *Adv. Enzyme Regul.* **50**, 375–399 (2010).

1344 51. Rai, R. *et al.* BRIT1 regulates early DNA damage response, chromosomal
1345 integrity, and cancer. *Cancer Cell* **10**, 145–157 (2006).
1346 52. Houlard, M. *et al.* Condensin confers the longitudinal rigidity of chromosomes.
1347 *Nat. Cell Biol.* **17**, 771–781 (2015).
1348 53. Eichinger, C. S., Kurze, A., Oliveira, R. A. & Nasmyth, K. Disengaging the
1349 Smc3/kleisin interface releases cohesin from Drosophila chromosomes during
1350 interphase and mitosis. *EMBO J.* **32**, 656–665 (2013).
1351 54. Wood, J. L., Liang, Y., Li, K. & Chen, J. Microcephalin/MCPH1 associates with
1352 the condensin II complex to function in homologous recombination repair. *J.*
1353 *Biol. Chem.* **283**, 29586–29592 (2008).
1354 55. Li, Y. *et al.* The structural basis for cohesin–CTCF-anchored loops. *Nature*
1355 **578**, 472–476 (2020).
1356 56. Chan, K. L. *et al.* Pds5 promotes and protects cohesin acetylation. *Proc. Natl.*
1357 *Acad. Sci. U. S. A.* **110**, 13020–13025 (2013).
1358 57. Srinivasan, M. *et al.* Scc2 counteracts a wapl-independent mechanism that
1359 releases cohesin from chromosomes during G1. *Elife* **8**, 1–34 (2019).
1360 58. Lee, B. G. *et al.* Cryo-EM structures of holo condensin reveal a subunit flip-flop
1361 mechanism. *Nat. Struct. Mol. Biol.* **27**, 743–751 (2020).
1362 59. Kong, M. *et al.* Human Condensin I and II Drive Extensive ATP-Dependent
1363 Compaction of Nucleosome-Bound DNA. *Mol. Cell* **79**, 99-114.e9 (2020).
1364 60. Golfier, S., Quail, T., Kimura, H. & Brugués, J. Cohesin and condensin extrude
1365 DNA loops in a cell-cycle dependent manner. *Elife* **9**, 1–34 (2020).
1366 61. Kim, Y., Shi, Z., Zhang, H., Finkelstein, I. J. & Yu, H. Human cohesin compacts
1367 DNA by loop extrusion. *Science (80-.).* **366**, 1345–1349 (2019).
1368 62. Collier, J. E. *et al.* Transport of DNA within cohesin involves clamping on top of

engaged heads by SCC2 and entrapment within the ring by SCC3. *Elife* **9**, 1–36 (2020).

63. Higashi, T. L. *et al.* A Structure-Based Mechanism for DNA Entry into the Cohesin Ring. *Mol. Cell* **79**, 917-933.e9 (2020).

64. Shi, Z., Gao, H., Bai, X. & Yu, H. Cryo-EM structure of the human cohesin-NIPBL-DNA complex. **1459**, 1454–1459 (2020).

65. Rao, S. S. P. *et al.* Cohesin Loss Eliminates All Loop Domains. *Cell* **171**, 305-320.e24 (2017).

66. Ran, F. A. *et al.* Genome engineering using the CRISPR-Cas9 system. *Nat. Protoc.* **8**, 2281–2308 (2013).

67. Grimm, J. B. *et al.* A General Method to Improve Fluorophores Using Deuterated Auxochromes. *JACS Au* **1**, 690–696 (2021).

68. Rao, S. S. P. *et al.* A 3D map of the human genome at kilobase resolution reveals principles of chromatin looping. *Cell* **159**, 1665–1680 (2014).

69. Durand, N. C. *et al.* Juicer Provides a One-Click System for Analyzing Loop-Resolution Hi-C Experiments. *Cell Syst.* **3**, 95–98 (2016).

70. Durand, N. C. *et al.* Juicebox Provides a Visualization System for Hi-C Contact Maps with Unlimited Zoom. *Cell Syst.* **3**, 99–101 (2016).

71. Sanborn, A. L. *et al.* Chromatin extrusion explains key features of loop and domain formation in wild-type and engineered genomes. *Proc. Natl. Acad. Sci. U. S. A.* **112**, E6456–E6465 (2015).

72. Ball, G. *et al.* SIMcheck: A toolbox for successful super-resolution structured illumination microscopy. *Sci. Rep.* **5**, 1–12 (2015).

73. Rodermund, L. *et al.* Time-resolved structured illumination microscopy reveals key principles of Xist RNA spreading. *Science (80-.).* **372**, eabe7500 (2021).

74. Matsuda, A., Schermelleh, L., Hirano, Y., Haraguchi, T. & Hiraoka, Y. Accurate and fiducial-marker-free correction for three-dimensional chromatic shift in biological fluorescence microscopy. *Sci. Rep.* **8**, 1–3 (2018).

75. Kraus, F. *et al.* Quantitative 3D structured illumination microscopy of nuclear structures. *Nat. Protoc.* **12**, 1011–1028 (2017).

76. Roehrl, M. H. A., Wang, J. Y. & Wagner, G. A general framework for development and data analysis of competitive high-throughput screens for small-molecule inhibitors of protein-protein interactions by fluorescence polarization. *Biochemistry* **43**, 16056–16066 (2004).

77. Voulgaris, M. & Gligoris, T. G. A protocol for assaying the ATPase activity of recombinant cohesin holocomplexes. *Methods Mol. Biol.* **2004**, 197–208 (2019).

Figure 1

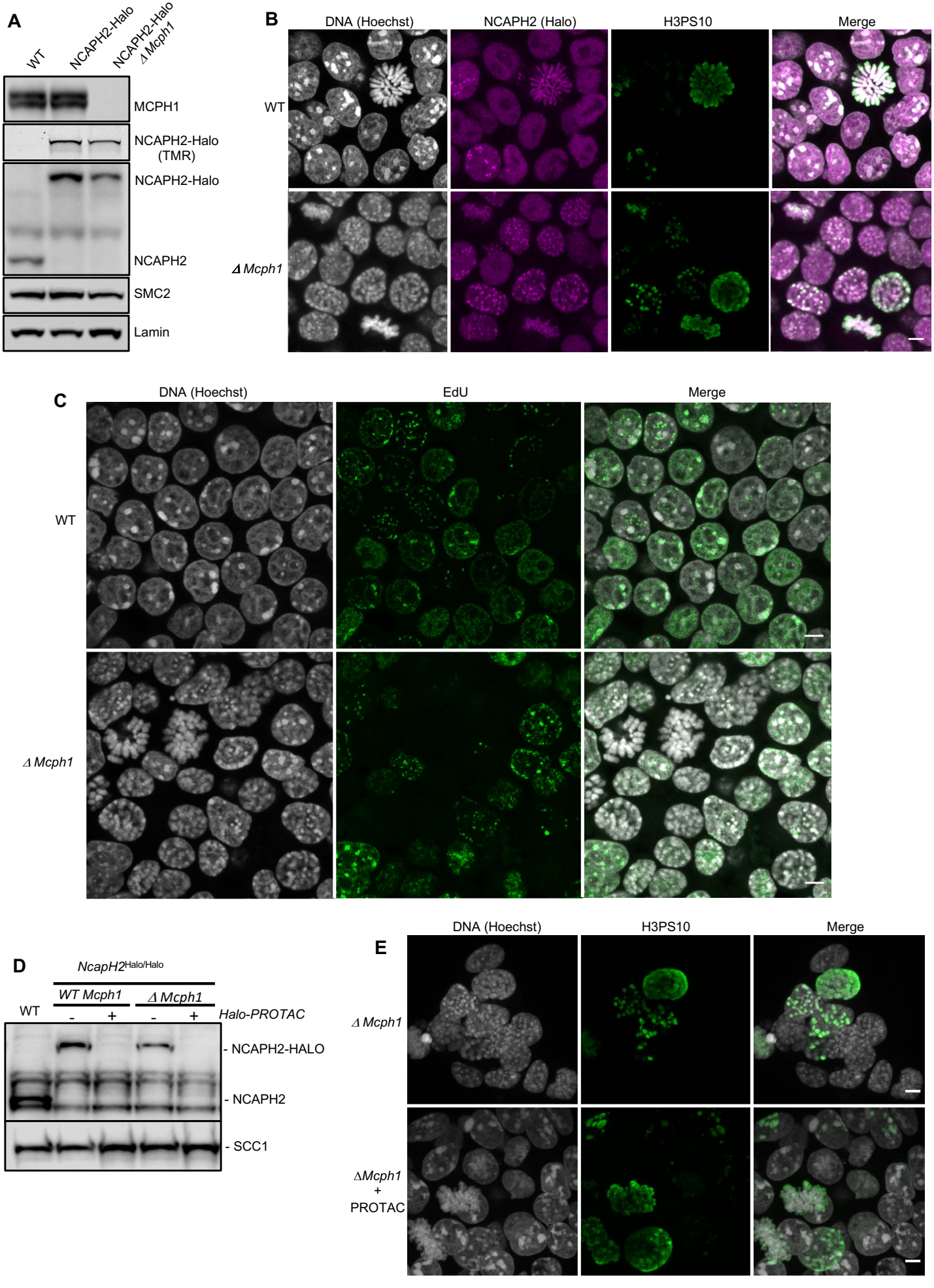

Figure 2

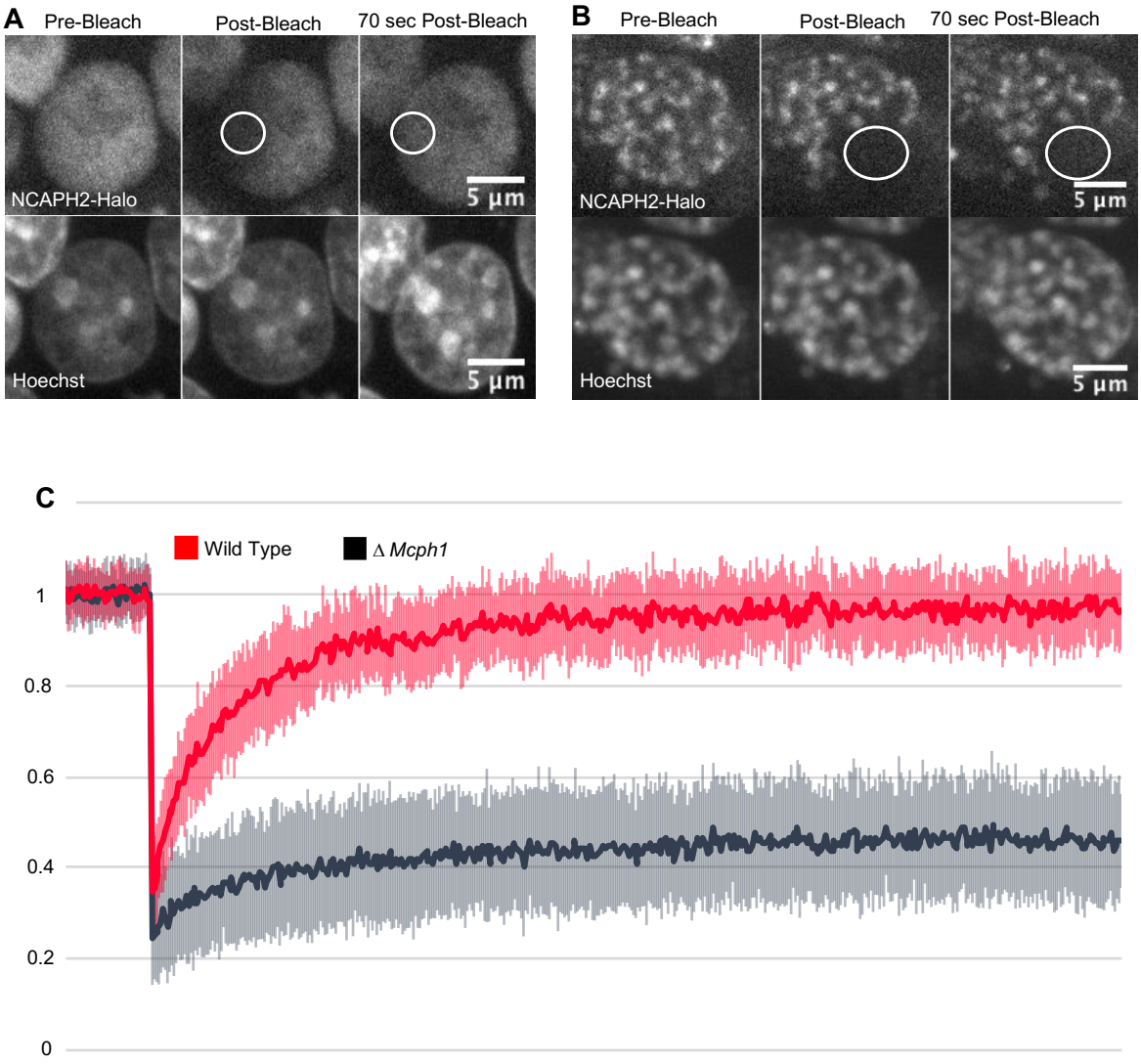

Figure 3

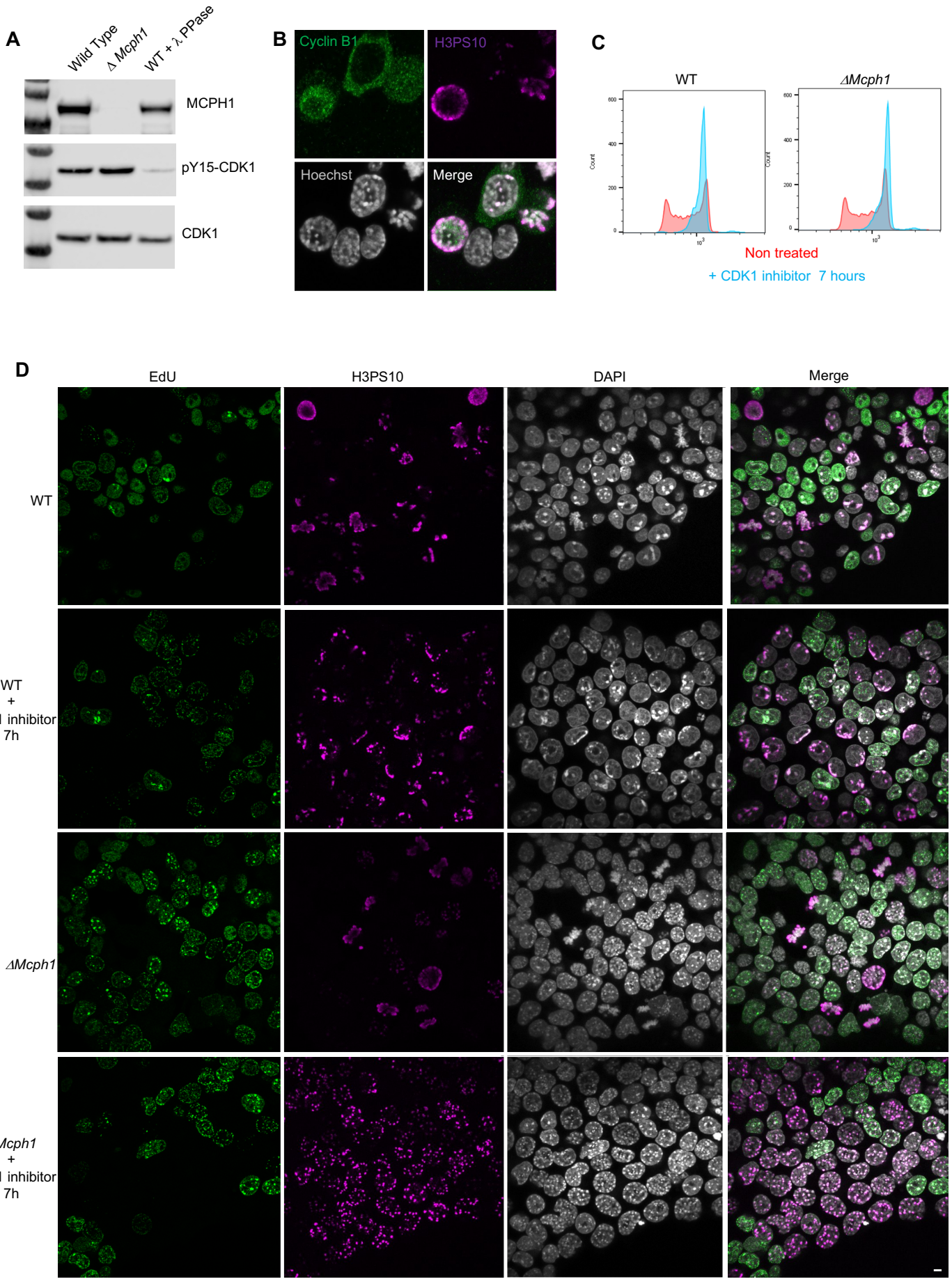

Figure 4

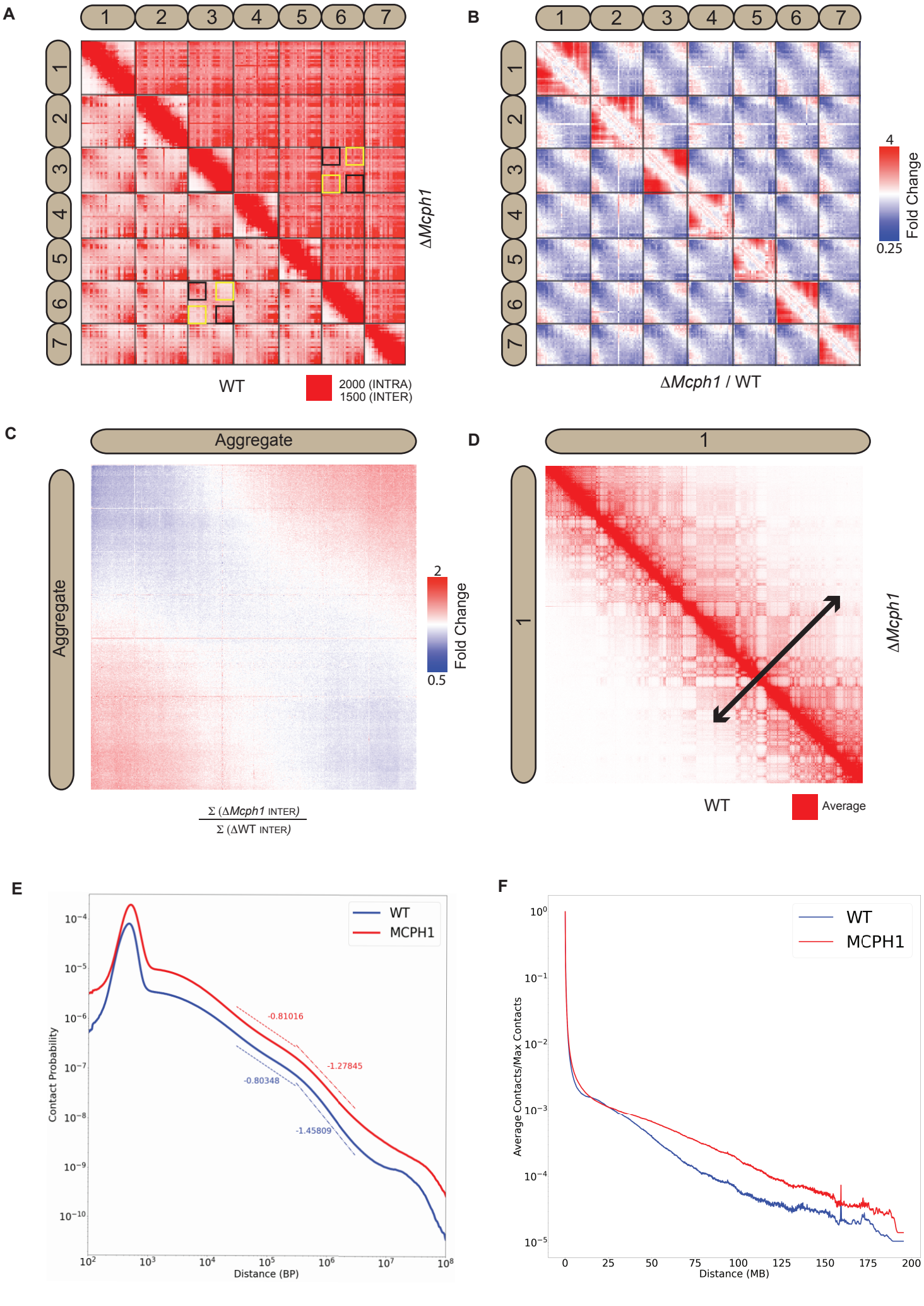

Figure 5

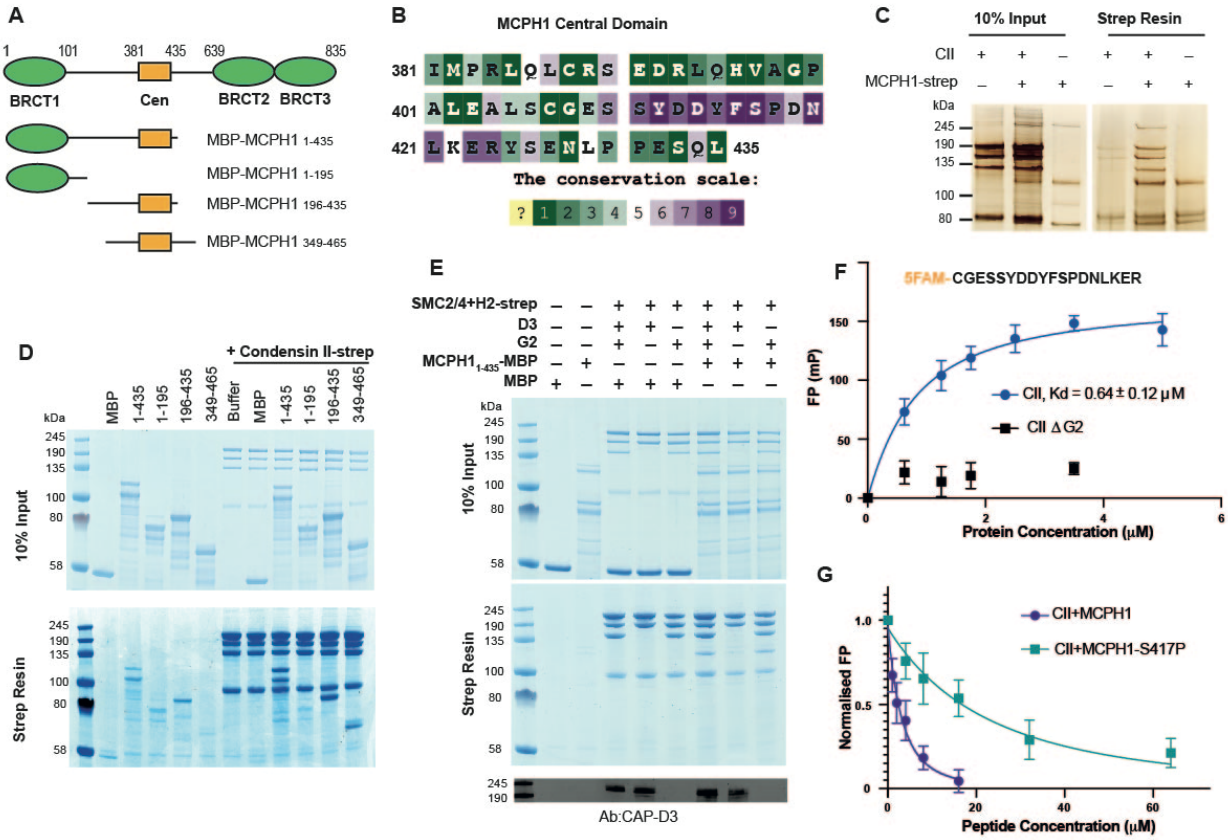

Figure 6

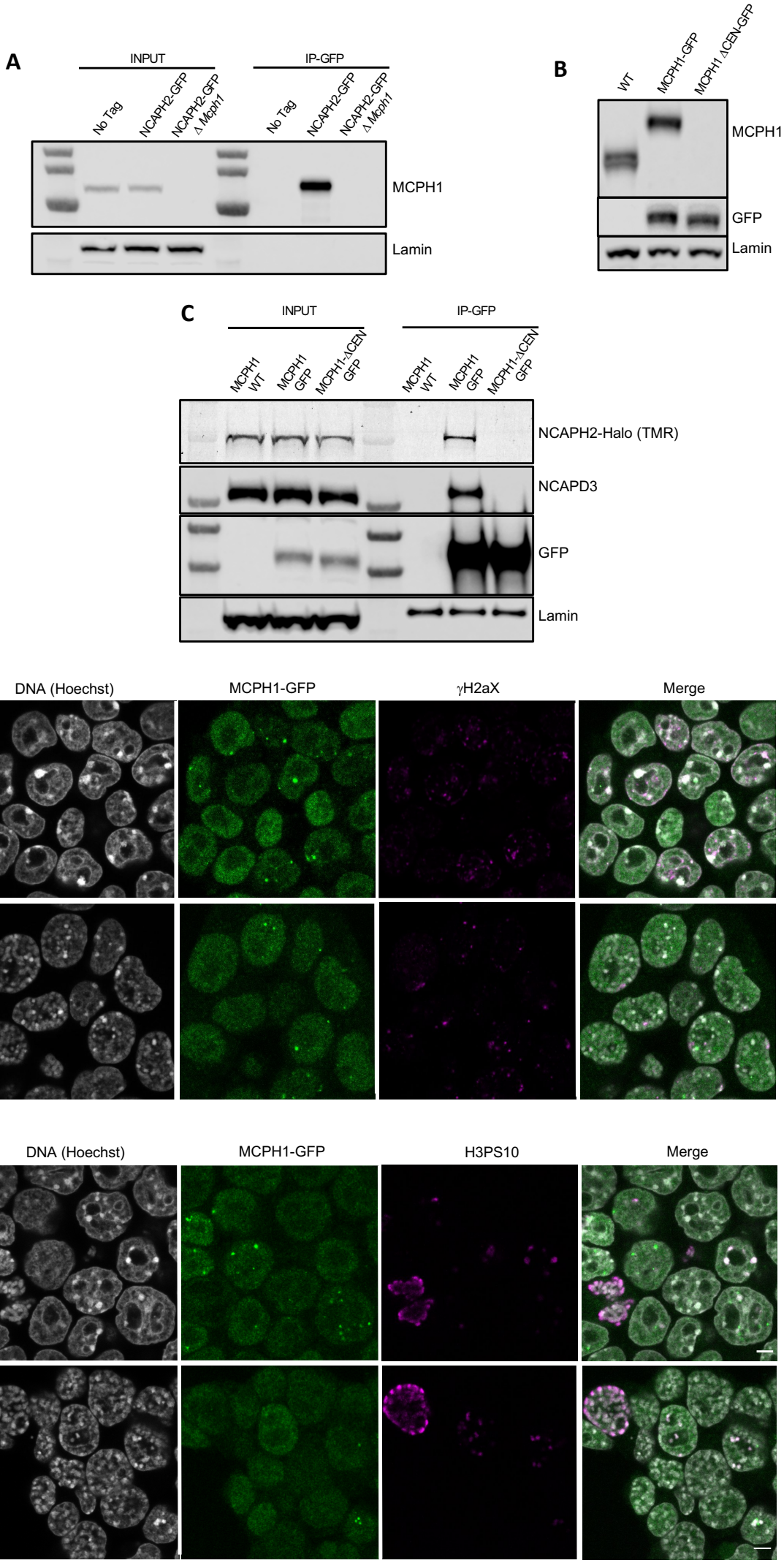

Figure 7

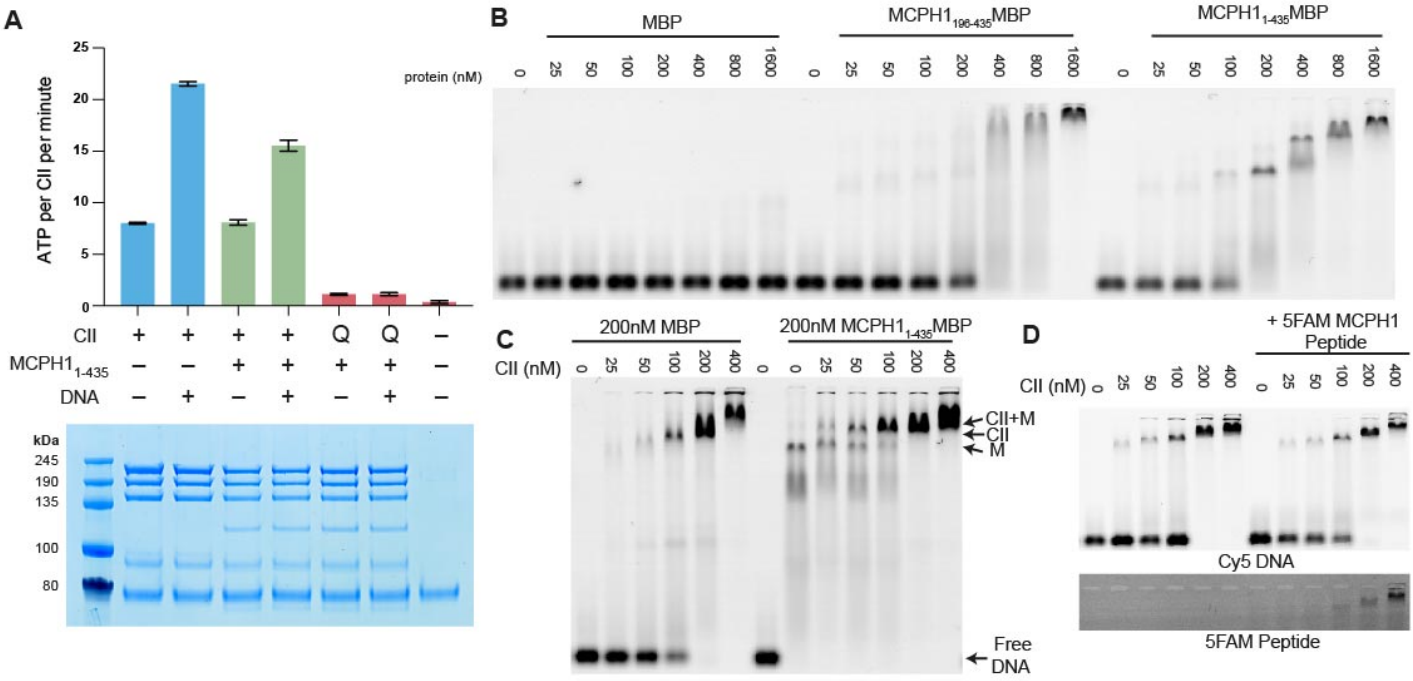

Figure 8

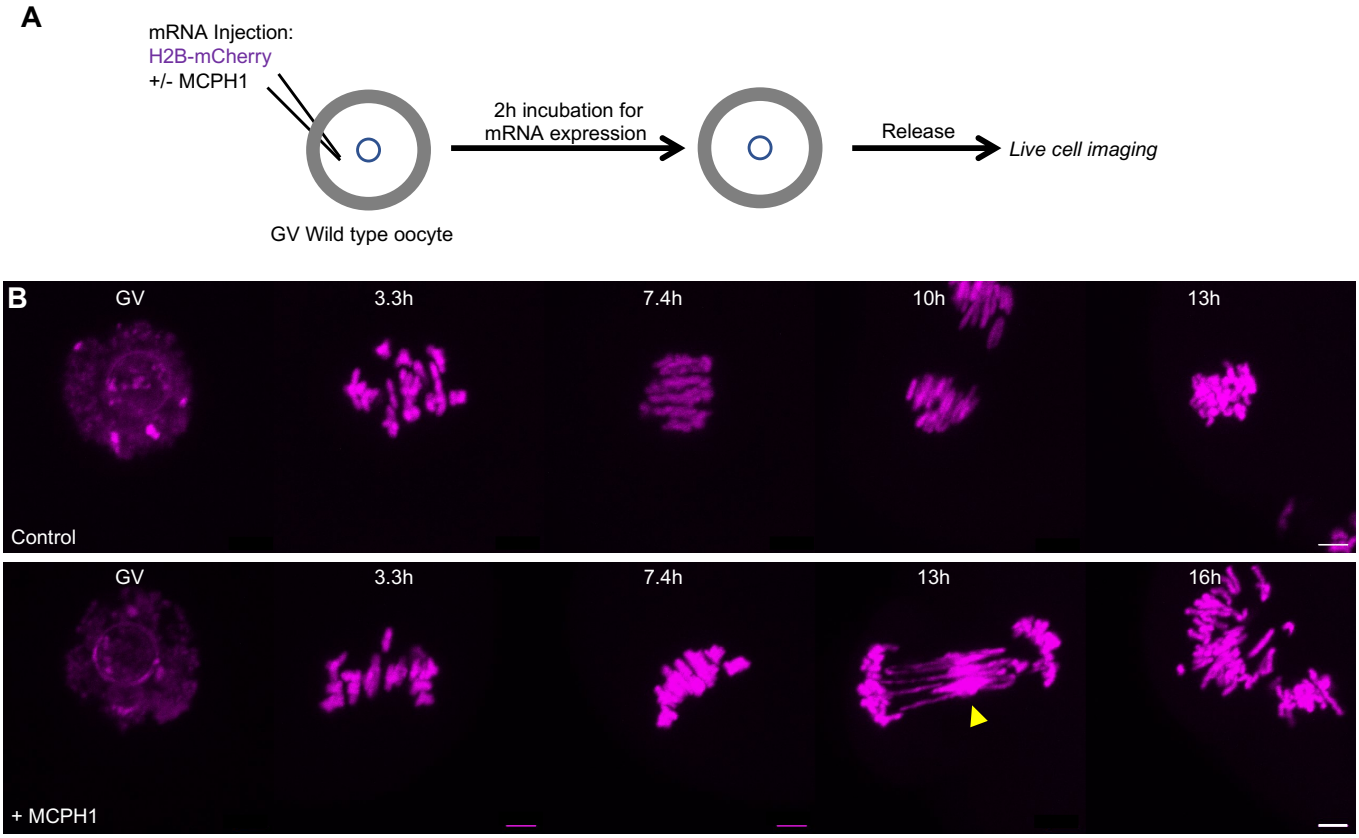

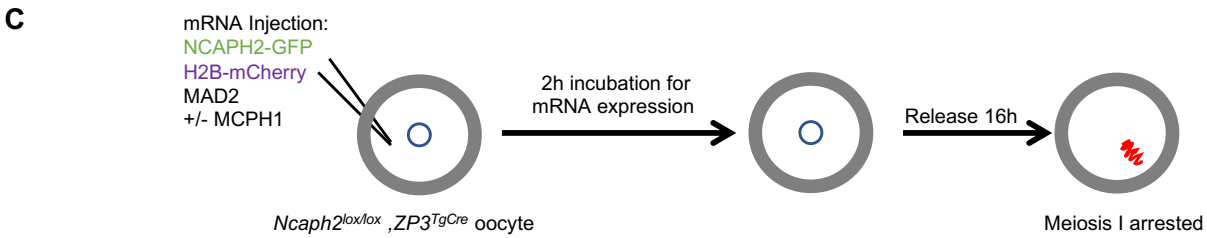

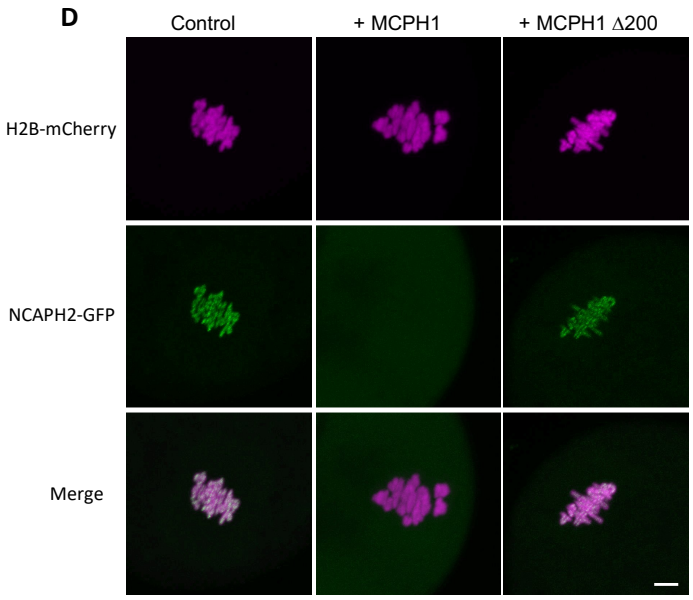

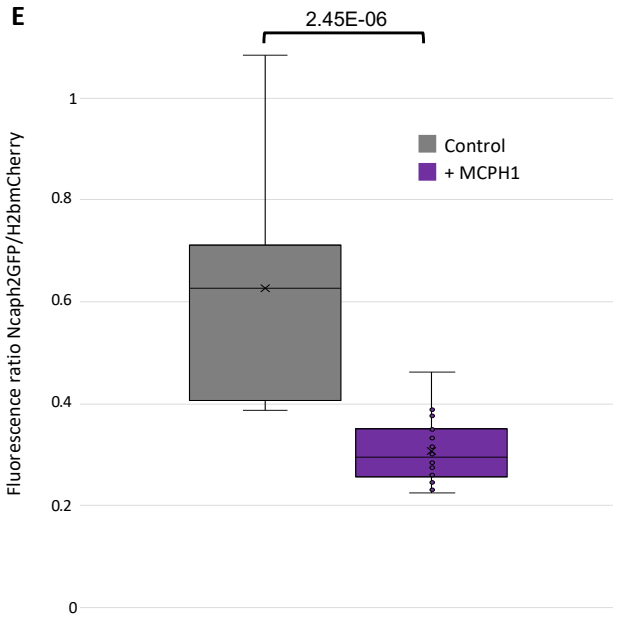

Figure 9

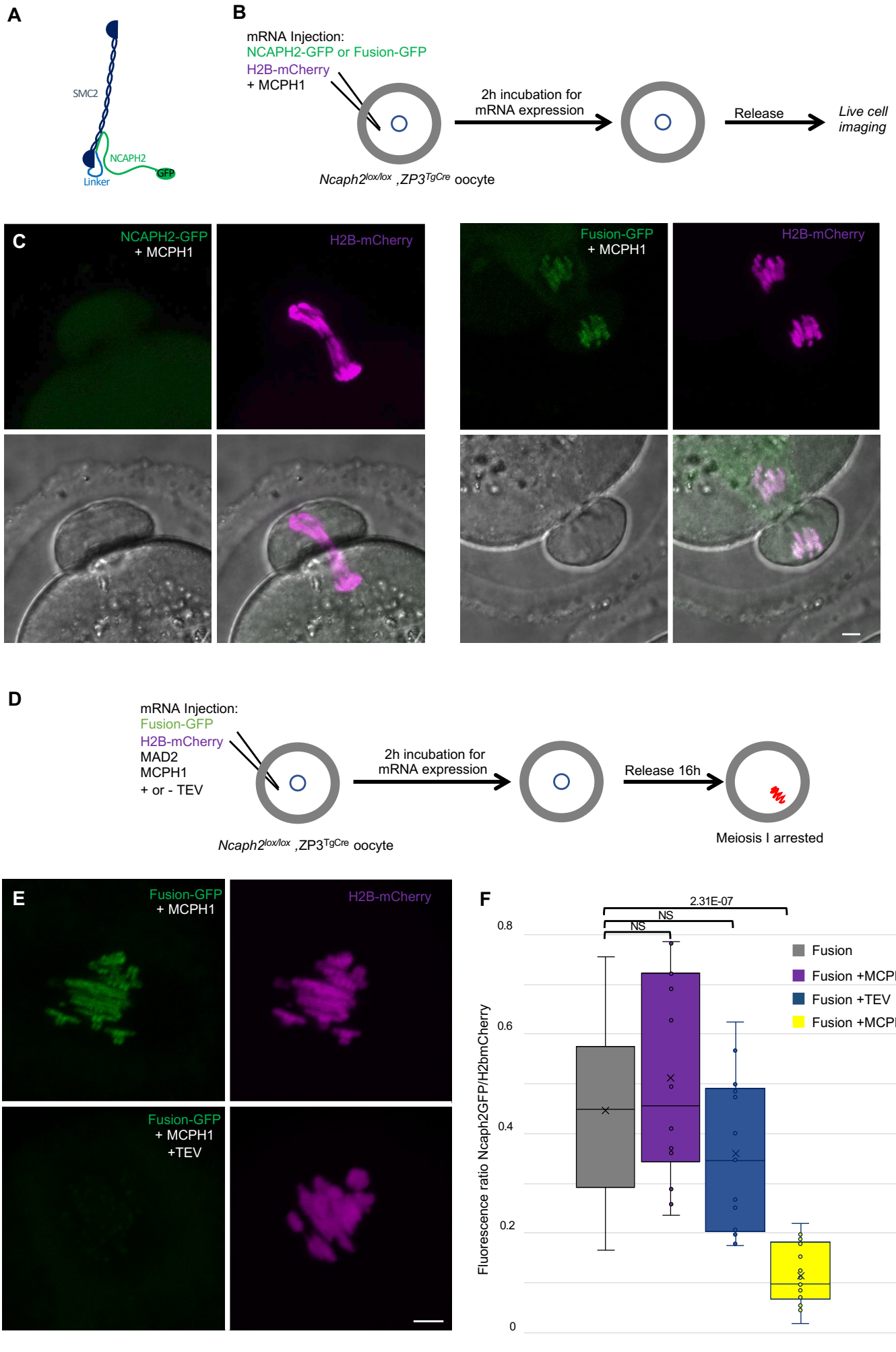

Figure 10

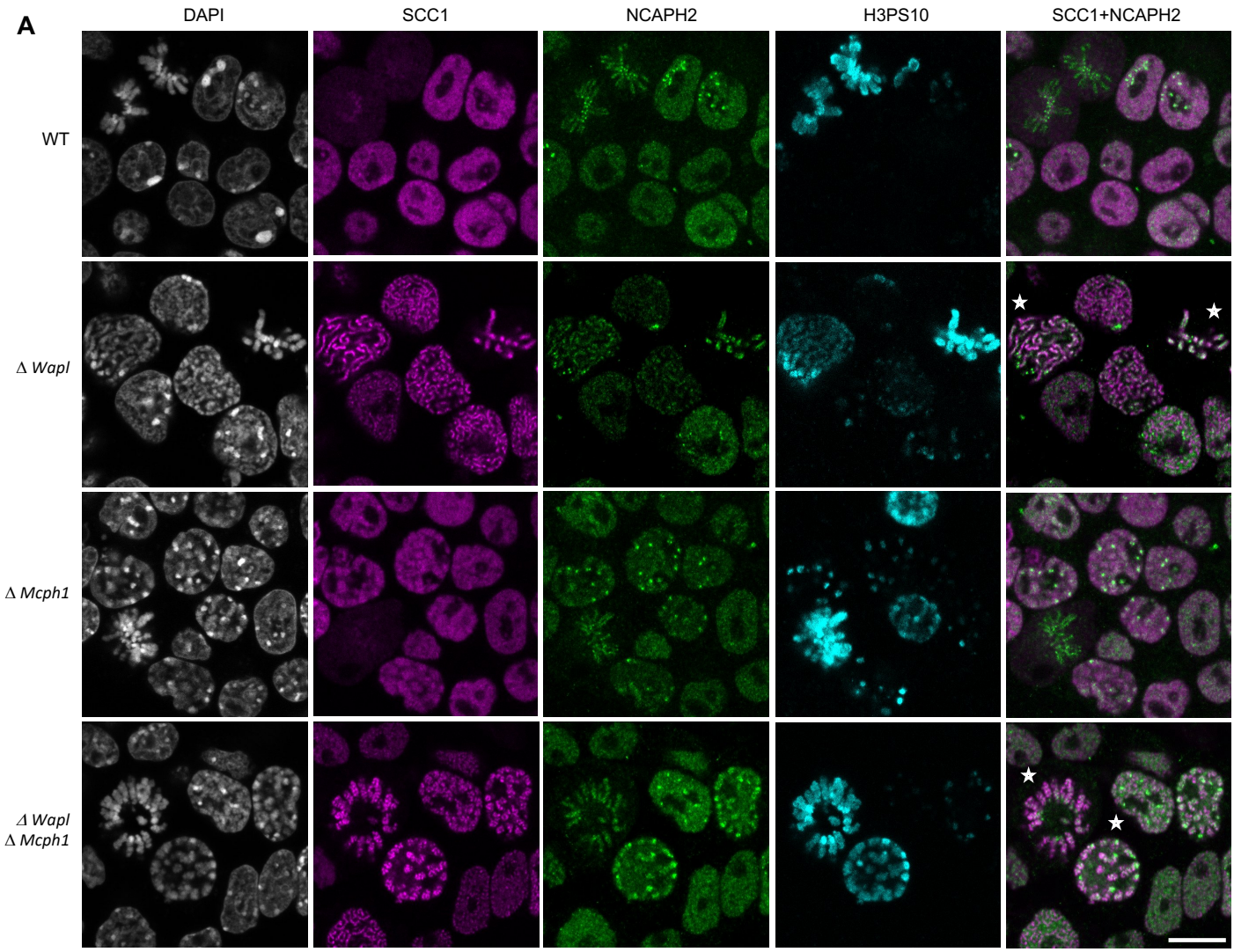

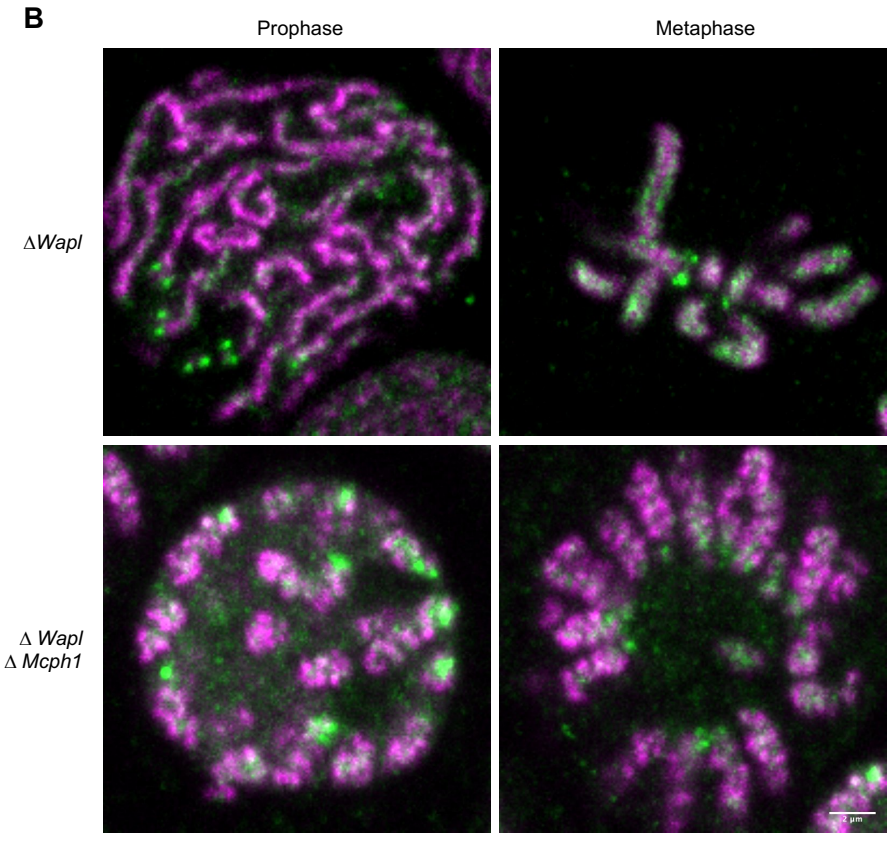

Figure 11

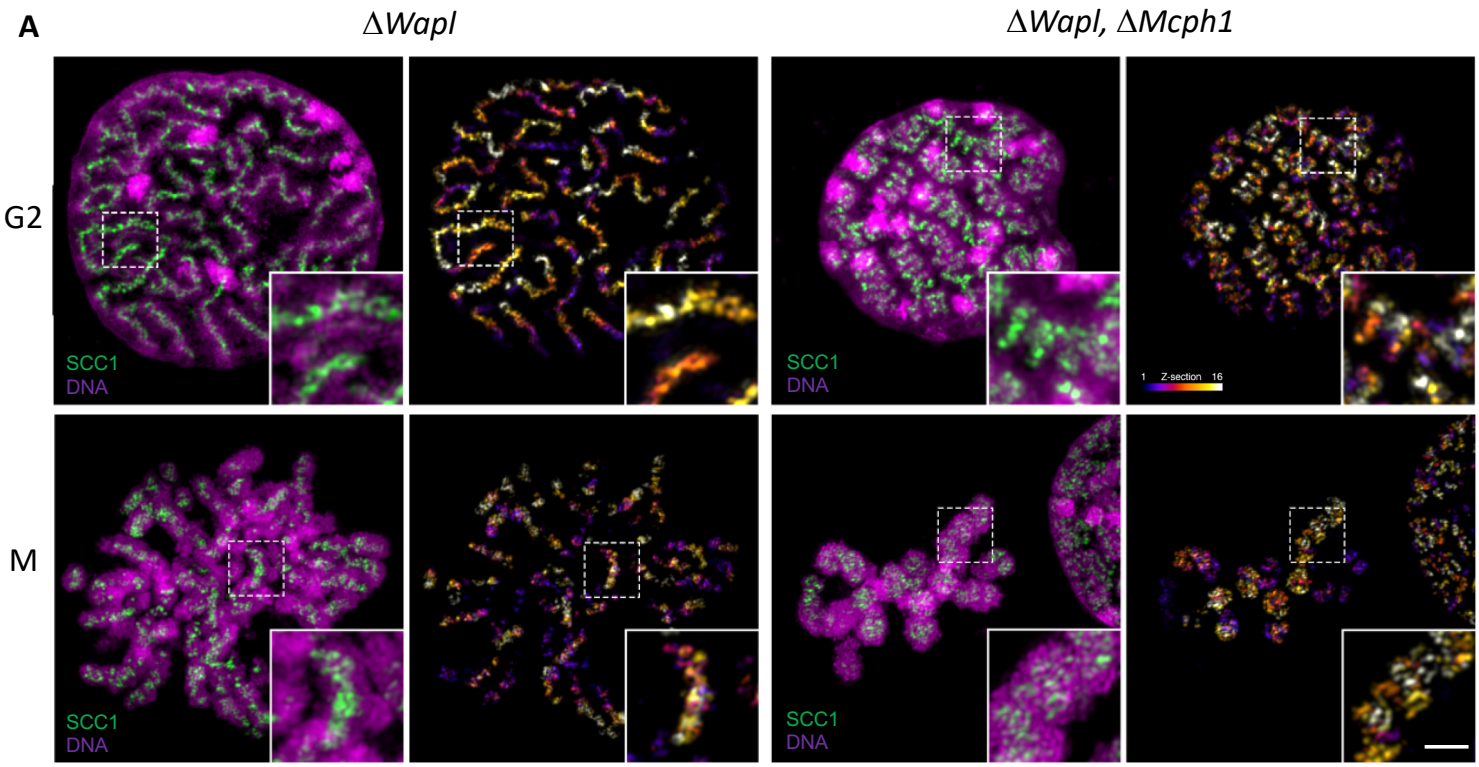

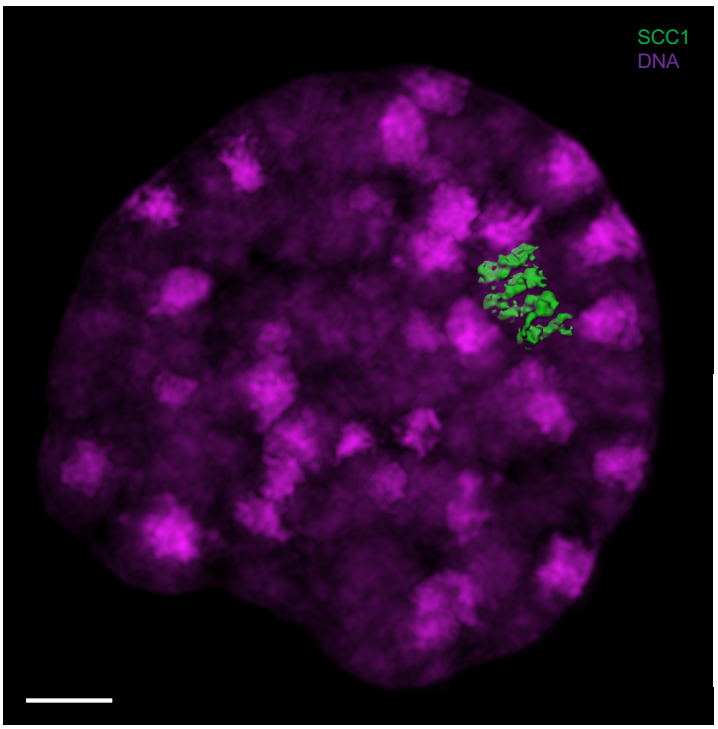

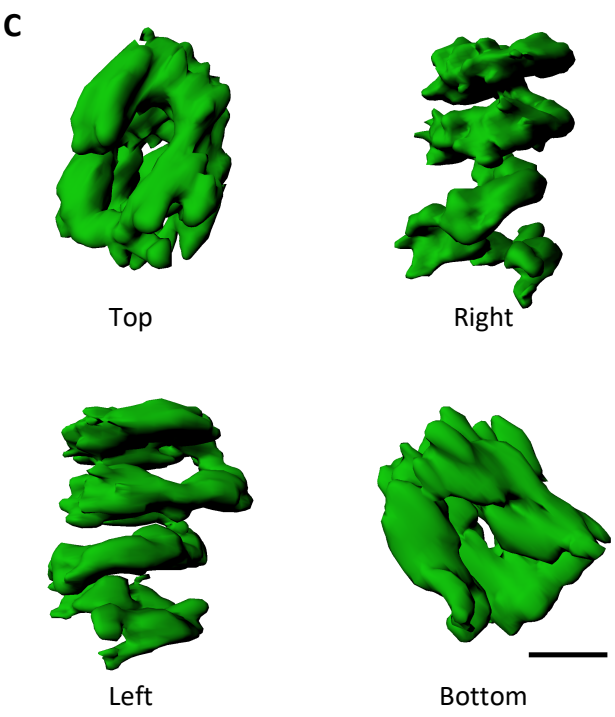

Supplementary Figure 1

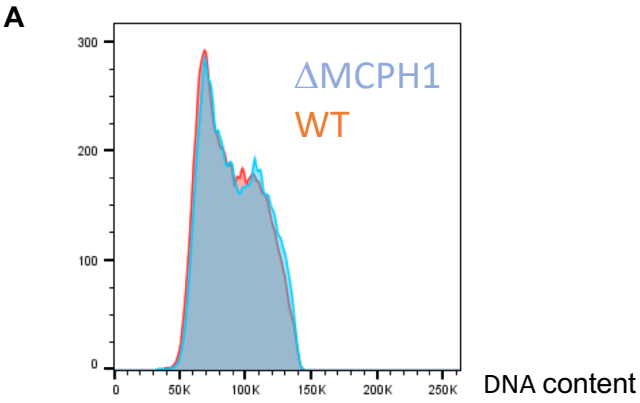

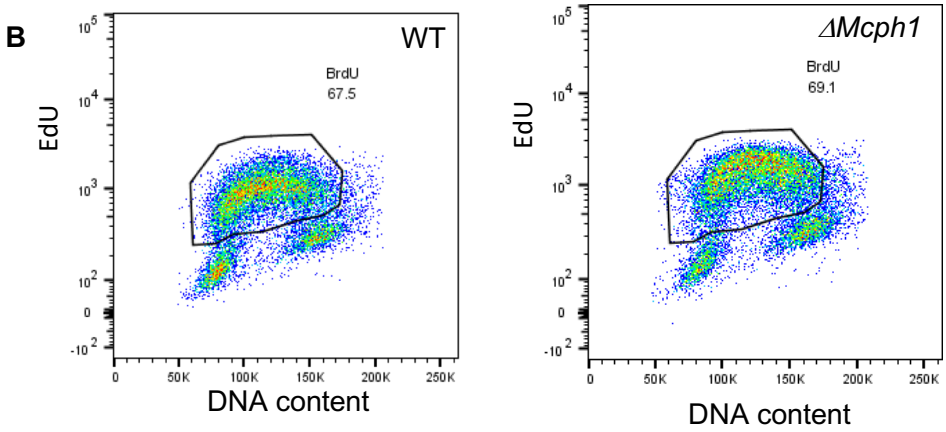

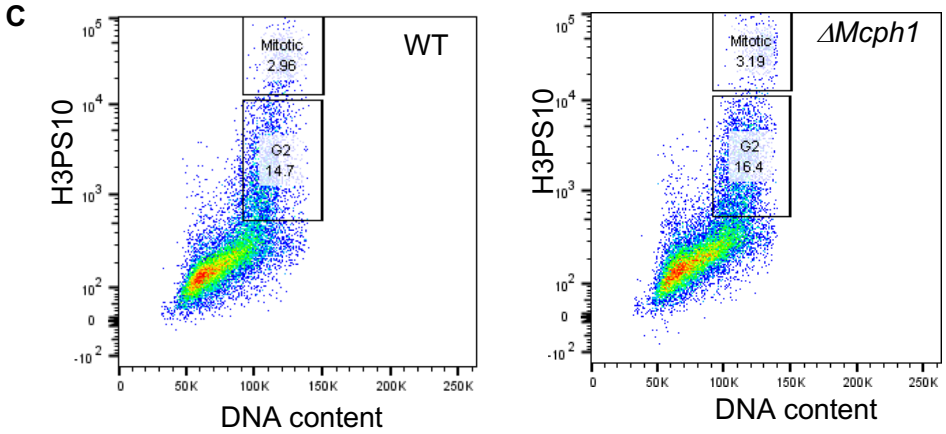

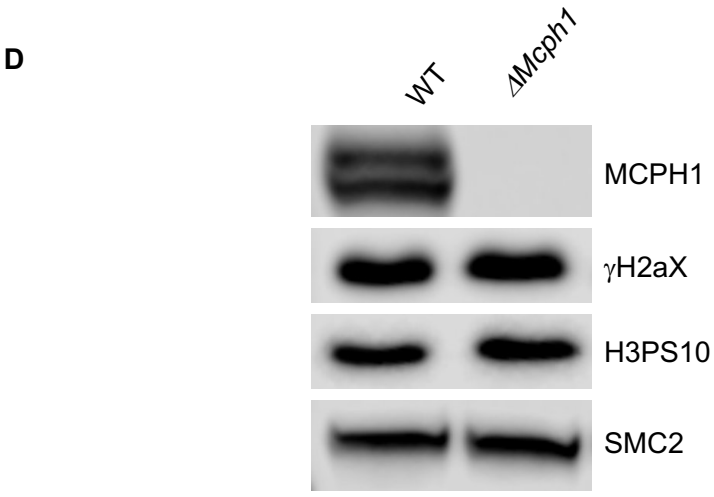

Supplementary Figure 2

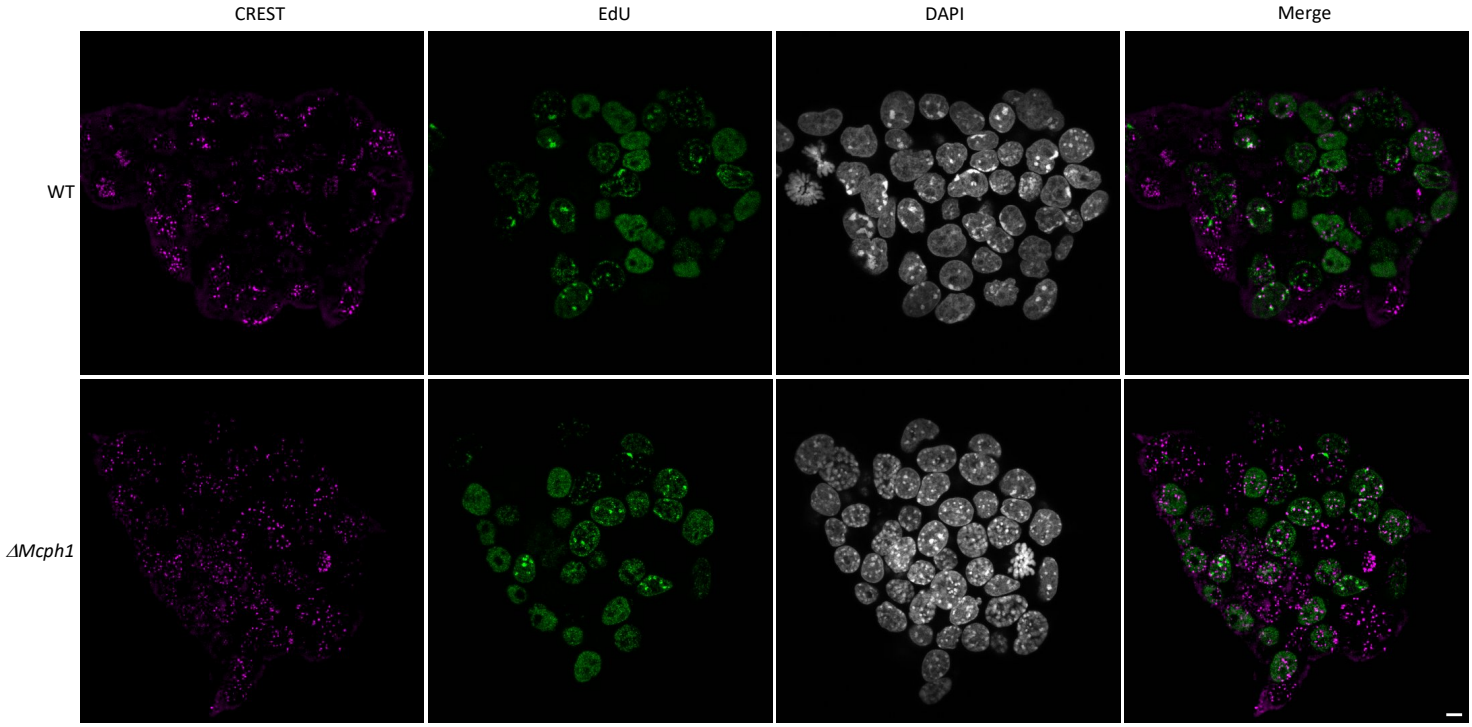

Supplementary Figure 3

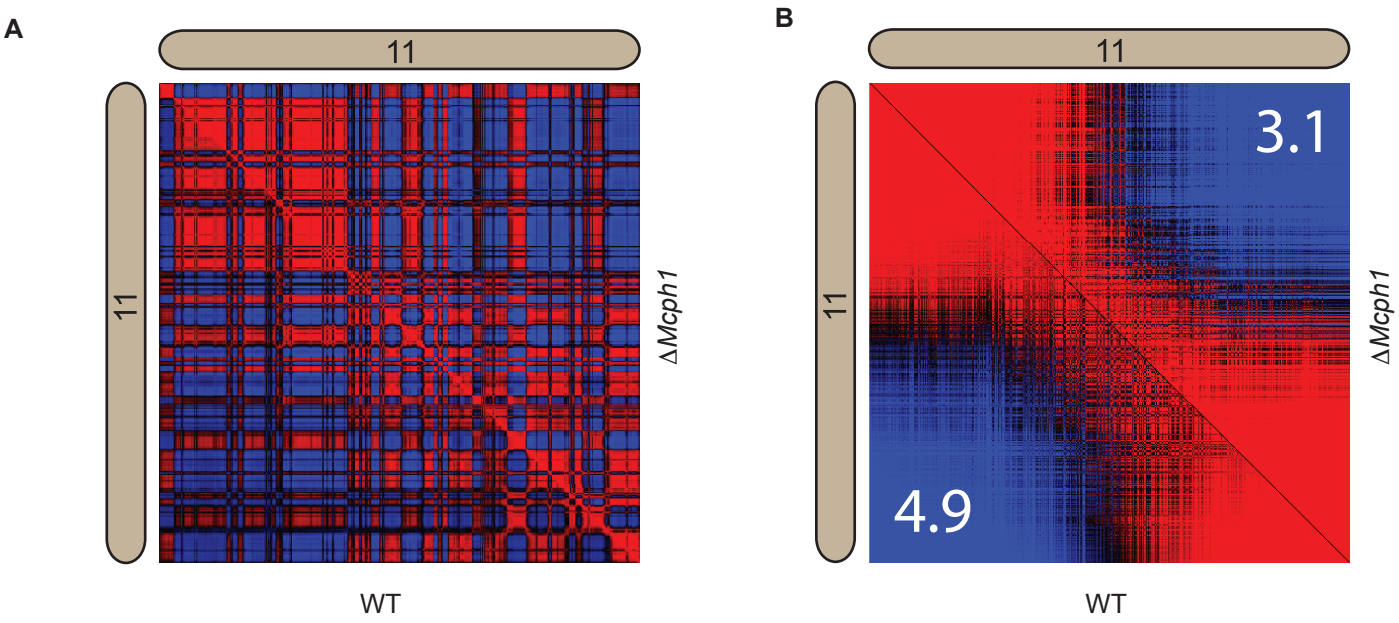

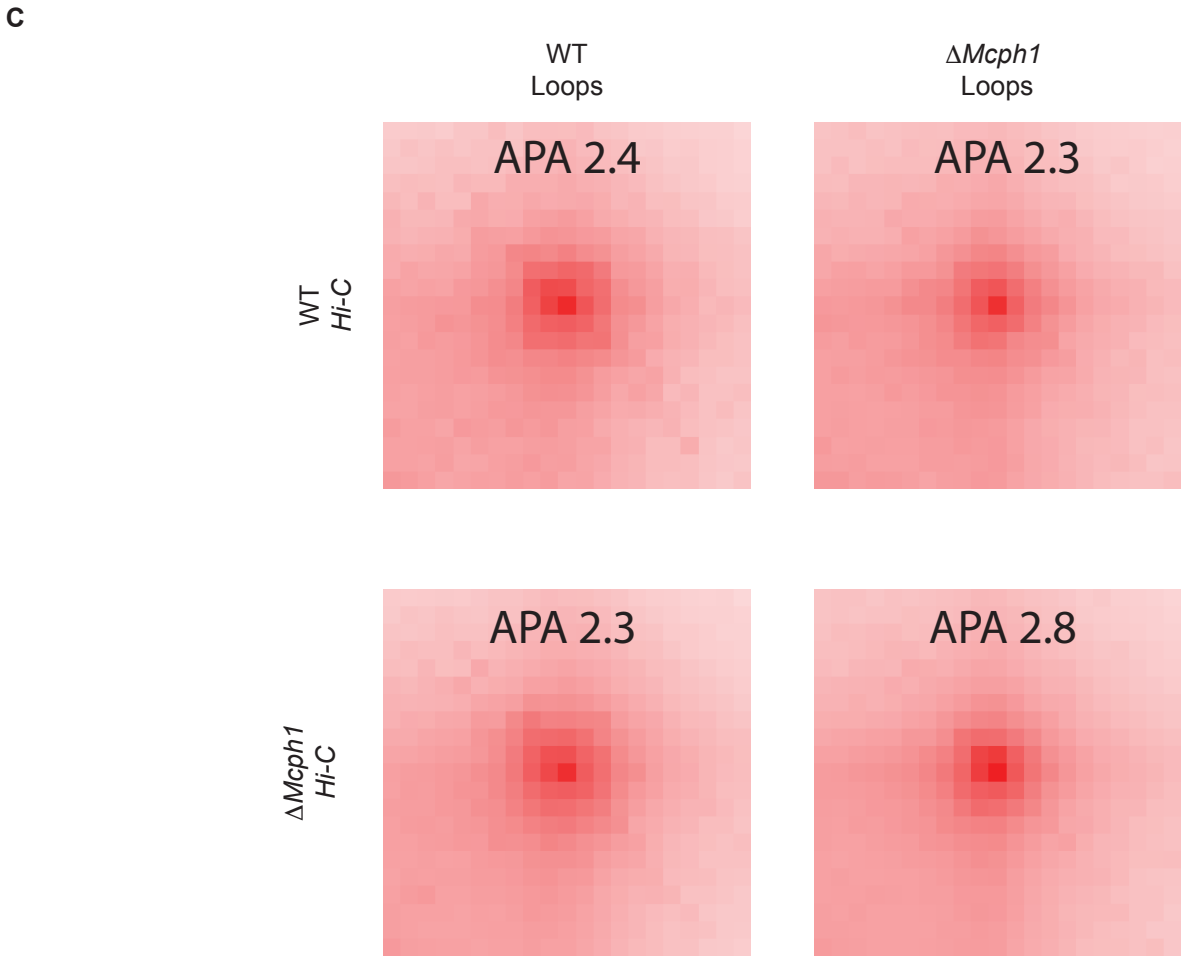

Supplementary Figure 4

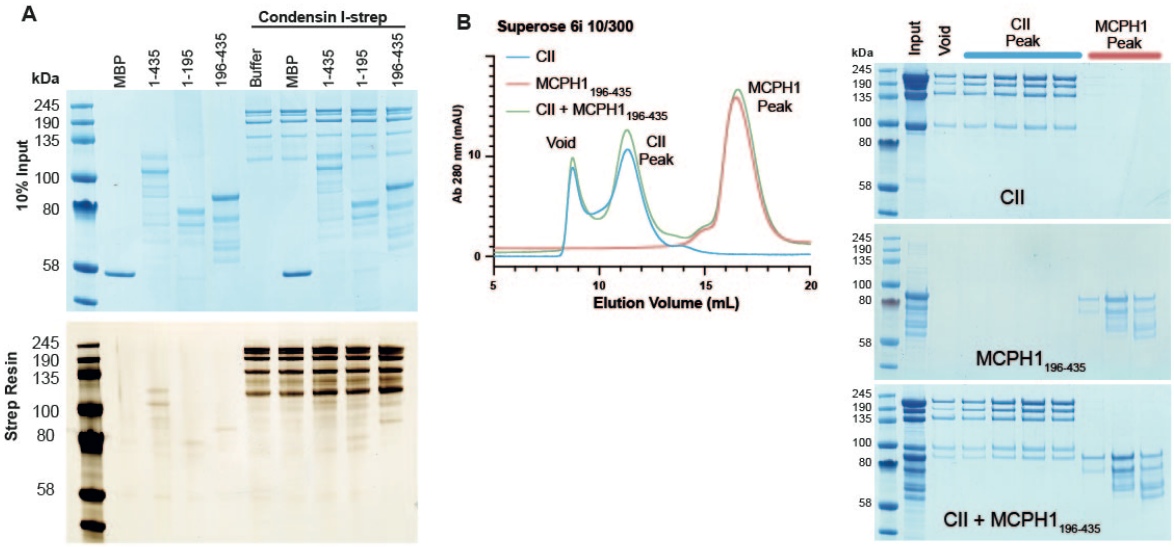

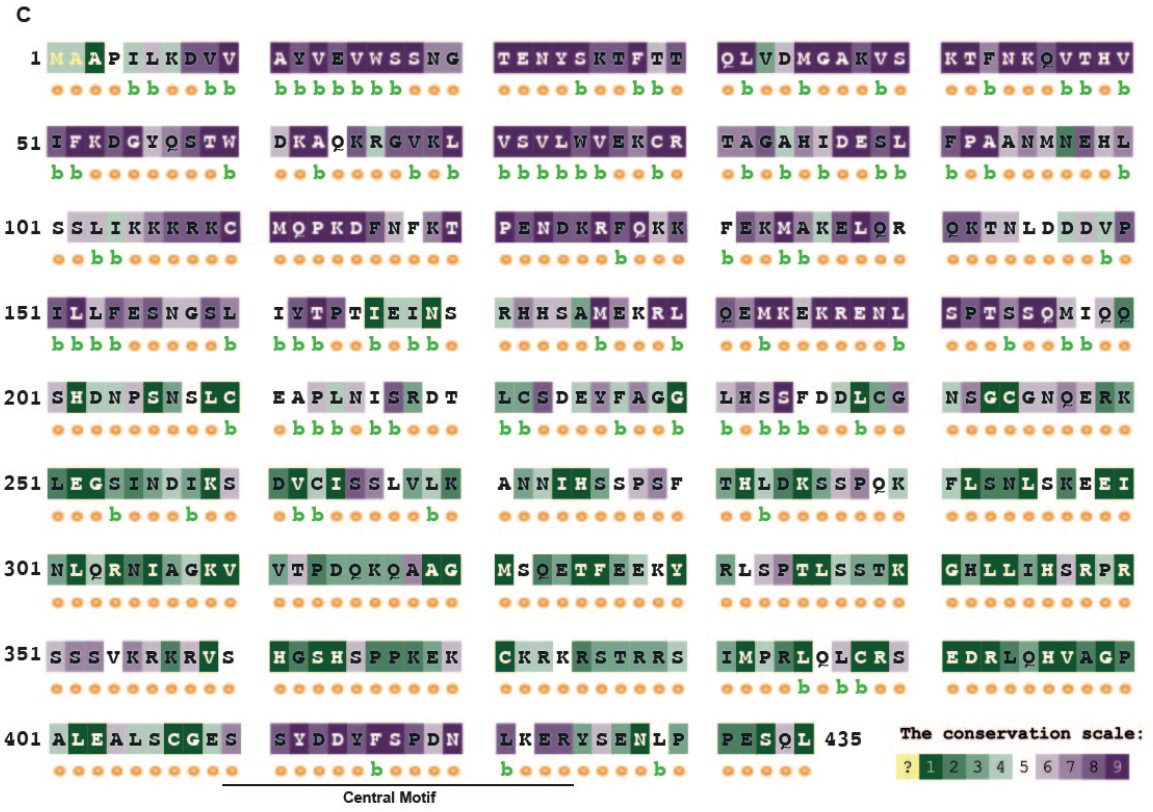

Supplementary Figure 5